2

University of Alabama
Bureau of Engineering Research
University, Alabama

MICROSTRIP TECHNOLOGY AND ITS APPLICATION
TO PHASED ARRAY COMPENSATION

Prepared by

James E. Dudgeon
Project Director

and

William D. Daniels
Research Associate

January 21, 1972

Submitted to

George C. Marshall Space Flight Center
National Aeronautics and Space Administration
Huntsville, Alabama

University of Alabama
Bureau of Engineering Research
University, Alabama

MICROSTRIP TECHNOLOGY AND ITS APPLICATION

TO PHASED ARRAY COMPENSATION

Prepared by

James E. Dudgeon
Project Director

and

William D. Daniels
Research Associate

January 21, 1972

Technical Report Number 2
Contract NAS8-25894

Submitted to

George C. Marshall Space Flight Center
National Aeronautics and Space Administration
Huntsville, Alabama

TABLE OF CONTENTS

i

CONTENTS (Continued)   Page

ii

LIST OF FIGURES

iv

CHAPTER I

INTRODUCTION

This report is a systematic analysis of mutual coupling compensation using microstrip techniques. A method for behind-the-array coupling of a phased antenna array has been reported by Hannan [13] and this method is investigated as to its feasibility. Beginning with a detailed review of microstrip transmission line parameters and fabrication techniques this report trys to prepare the reader fo an in-depth realization of Hannan's procedure using typical component values. The matching scheme is tried on a rectangular array of $\lambda/2$ dipoles, but it is not limited to this array element or geometry. In the example cited the values of discrete components necessary were so small an L-C network is needed for realization. Notice that such L-C tanks might limit an otherwise broadband array match, however, this is not significant for this dipole array. Other areas investigated were balun feeding and power limits of spiral antenna elements. Hannan's method requires a knowledge of the parameters of each element in an active array environment. Experimental attainment of these values could be expensive whereas computer simulation would be quick and precise. This method is not cost competitive with some of the matching schemes such as dielectric cover sheets, however, future advances in batch processing may amend this. Assuming adequate precautions, post processing would lower cost by increasing yield. The redeeming feature of this method is its theorethical ability to match preciesly every element individualy, whereas the other wide angle

1

impedance matching techniques attack the problem macroscopicly.

Chapter II delves into the theory and realizations of stripline and microstrip. These transmission lines have been widely used in industry and an abundance of information on them is available in literature. Other types of transmission lines presently under study are the coplanar wave guide and slot line. These t-lines would allow shunt mounting of devices without drilling holes in the substrate. Stripline (known as slab line or triplate) is constructed of a dielectric supported center conductor sandwiched between two ground planes and is thus self shielded. Microstrip which consists of a ribbon conductor over a ground planes is not self shielded so it is usually enclosed in a metal box to curb radiation exchanges. The parameter of characteristic impedance is considered in detail and sufficient information is included for any design implementation. In the propagation of quasi-TEM waves, because the fringe fields above the microstrip are in air which has a relative permittivity of one, the conductor supported by a dielectric appears to have an effective dielectric constant lower than the value for the dielectric. The phase velocity and characteristic impedance of stripline are functions of the dielectric in which the conductor is embeded. Microstrip properities are determined by a knowledge of ε'_r, the effective value of the dielectric constant. The fields of closely spaced t-lines interact producing a mutual coupling which has found uses in filters, delay lines, and directional coupler. Graphs are illustrated which allow the interpolation of characteristic impedance for even and odd mode coupling. The majority of the developments in Chapter II pertain to microstrip because it

seems the most likely candidate for integrated system work at microwave frequencies. Active devices and passive systems can be built directly into the microstrip. Microstrip requires less area and is less expensive to fabricate than the alternate transmission line realizations.

Chapter III presents some techniques for microwave integrated circuit design and fabrication. Substrates, conductors, and dielectrics are evaluated and conclusions as to the most optimum choices are stated. Presently elements for microwave circuits are categorized as either lumped or distributed. Lumped element performance is independent of frequency over the range of interest while distributed elements are sensitive to frequency. The lumped element approach is best suited to direct, electrical coupling between adjacent antenna elements because it is frequency independent and assures braodbandness in impedance matching. For an element to remain truly lumped its circuit components must be electrically much shorter than a wavelength so for the frequency range of interest the geometry is minute. Because of the simple formulations for finding inductance values (purely geometric: a ribbon of conductor in free space) and capacitances (proportional to area for a given separation and dielectric constant), the lumped element design is largely concerned with fabrication guidelines for the devices. Photolithographic fabrication has made it possible to produce lumped elements to X-band and lower K_u band. These lumped elements because of their size, can be reproduced inexpensively with many circuits on a single substrate. Lumped element MIC's are readily compatible with solid-state devices. Alunmina (Al_2O_3) has become a widely used

substrate because it has a low loss tangent and high dielectric constant (order of 10). Pure sapphire would be preferred since its loss tangent is lower, but it is fairly expensive. In order to reduce line losses further the conductor should be chemically bonded to the substrate. A mechanical bond requires a rough substrate which will increase line loss. Two production techniques for lumped and distributed elements are reviewed. Thin film processing which allows very high resolution on the etch of the pattern has a lower dc resistance than the thick film method. With thick film processing, however, capacitors capable of handling high voltages and having no pinholes are easier to make. Microwave resistors result from films and conductors of known sheet resistance. The quality factor of the lumped elements decreases greatly at frequencies above 8 GH_z with present technology, even though higher Q's are predicted by theory. The total Q is dependent on the conductor Q and the dielectrics loss tangent (i.e. zero loss tangent implies infinite Q_d). Two approaches to fabrication of these circuits are hybrid and monolithic integration. In the monolithic circuit active elements are grown epitaxially in pockets of the substrate. To date silicon has proved unsucessful as a substrate because it fails to keep is resistivity. Galium arsenide would be a better choice, but the technology involved with monlithic fabrication is furturistic.

The intent of this report is to investigate all facets of Hannan's method for wide scan impedance matching a planar phased array. Chapter IV is concerned with a method to effect impedance matching through behind-the-array interconnecting circuits. The hybrid combination

of lumped and distributed elements would be the most optimum approach
to realization. Here, the lumped elements would be used to realize the
behind-the-array mutual coupling and the distributed or microstrip
transmission line will connect these circuits to the antenna elements.
The method of Hannan for interconnecting circuits is adopted and this
method is compared with other schemes for array matching. The dielectric
cover sheet utilizes mutual coupling to effectively connect every
element of the array and if properly designed allows an approximate
impedance match. An example is worked out using Hannan's procedure and
once the values of the components are determined, their fabrication
is discussed as to feasibility. Once the circuits are produced there
may arise a need to tune and fine adjust them. Initial design should
allow for post fabrication improvements. Some of these are micro
cantilever for tuning microstrip and trimming metal from lumped
elements. The optimum array geometry in terms of aperture size per
number of elements if the triangular grid. Six interconnecting
circuits would be required as opposed to only four for the retangular
geometry, however, there is no appreciable difference in the matching
requirements if a dielectric cover sheet were used.

Chapter V deals with fabrication problems, balun design, and power
limits associated with spiral antenna elements. Because the spiral
antenna which is a balanced, symmetrical structure is to be fed with
microstrip, an unbalanced transmission line, and interface between
them is needed. Assuming the spiral antenna is to be used in a
wideband mode, the interface is hopefully frequency independent.

This chapter describes two different baluns which are applicable to the spiral. The Bawer balun is commonly used in cavity-backed spirals, while a balun which employs coupled microstrip phase shifters seems the best suited for K_u-band spiral arrays because its ground plane can serve as the spiral's ground plane. Also the later balun provides matching at the center frequency whereas the Bawer balun does not. The maximum power the antenna can radiate was investigated. A value of four watts rms per element is cited considering a large safety factor. For spacecraft applications a thin layer of dielectric might be used to cover the spiral's surface to prevent voltage breakdown between the conductors since the breakdown in air is a function of pressure and ion density. At the frequencies considered it is concluded that the antenna is capable of radiating as much power as the sources can provide.

CHAPTER II

MICROSTRIP ANALYSIS TECHNIQUES

The use of microstrip and striplines in low price circuits of high reliability obviously requires knowledge of their microwave parameters in order to realize their design. This section is concerned with three methods of obtaining the capacitance associated with their geometries. For reliable conclusions it is necessary that for identical geometries the three different analytic methods yield the same or very close results. If the capacitance of a geometry is known, the characteristic impedance of the transmission line can be found if the effective dielectric constant of the separating medium is known. Mutual coupling between these lines is specified if it exists. The three methods to be discussed are: conformal mapping, iteration techniques, and variational methods.

A.   CONFORMAL MAPPING

A review of complex variables will serve as foundation for the following. A function $\Omega(w)$ of a complex variable $w = u + jv$ is called analytic within a region R if the derivative

$$\frac{d\Omega(w)}{dw} = \lim_{\Delta w \to 0} \frac{\Delta\Omega}{\Delta w}$$

exists within R independent of the direction chosen for Δw. The necessary and sufficient conditions for the above to hold are known as

7

the Cauchy-Riemann conditions. For

$$\Omega = \Phi + j\Psi \quad \text{(complex potential)}$$

$$w = u + jv$$

the Cauchy-Riemann conditions are

$$\frac{\partial \Phi}{\partial u} = \frac{\partial \Psi}{\partial v} \qquad \frac{\partial \Phi}{\partial v} = - \frac{\partial \Psi}{\partial u} \qquad (2\text{-}1)$$

Now

$$\frac{\partial}{\partial u}\frac{\partial \Phi}{\partial u} = \frac{\partial^2 \Phi}{\partial u^2} = \frac{\partial^2 \Psi}{\partial v \partial u} \qquad (2\text{-}2)$$

$$\frac{\partial}{\partial v}\frac{\partial \Phi}{\partial v} = - \frac{\partial^2 \Psi}{\partial u \partial v} = \frac{\partial^2 \Phi}{\partial v^2} \qquad (2\text{-}3)$$

Substituting (2-2) in (2-3) gives Laplace's equation

$$\frac{\partial^2 \Phi}{\partial u^2} + \frac{\partial^2 \Phi}{\partial v^2} = 0 \qquad (2\text{-}4)$$

A similar procedure will show that both Φ and Ψ are solutions to Laplace's equation. Thus we call Ω the complex potential. Φ(real part of Ω) are the lines of constant potential (to be shown) and Ψ(imaginary part of Ω) are the lines of constant field strength (electric flux).

The Schwarz-Christoffel transformation gives a method by which the interior of a polygon in one complex plane can be mapped onto the upper half of another complex plane. It is given by

$$\frac{dz}{dw} = A'(w-x_1)^{(\frac{\alpha_1}{\pi} - 1)}(w-x_2)^{(\frac{\alpha_2}{\pi} - 1)}(w-x_3)^{(\frac{\alpha_3}{\pi} - 1)} \qquad (2\text{-}5)$$

where

x_i = point on u-axis of w-plane corresponding to point in z-plane

α_i = corresponding to angle traversed in z-plane when x_i in w-plane is traversed.

Consider two parallel, semiinfinite conductors in the z-plane.
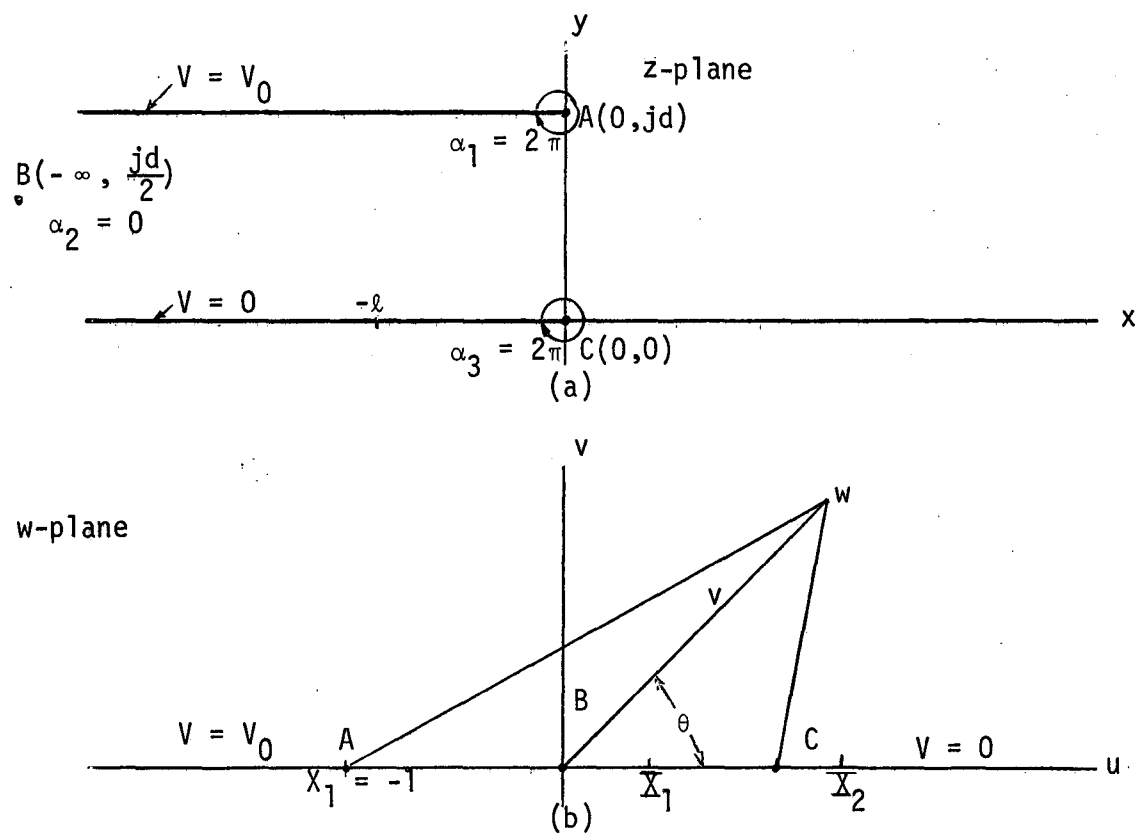
Fig. 2-1. Complex Plane Geometries.

From inspection of the two planes the transformation can be written by (2-5) to be

$$\frac{dz}{dw} = A' \frac{(w+1)^{1}(w-1)^{1}}{w} = A' \frac{(w^2-1)}{w} = A'w - \frac{A'}{w} \qquad (2\text{-}6)$$

$$Z = \int \frac{dz}{dw} \, dw = A' \frac{w^2}{2} - A' \, \ln w + B' \qquad (2\text{-}7)$$

Applying the transformation condition at point C says when z = 0   w = 1

$$0 = \frac{A'}{2} + B' \qquad (2\text{-}8)$$

yielding

$$B' = -\frac{A'}{2} \qquad (2\text{-}9)$$

Applying transformation condition at point A says when z = jd   w = -1

$$jd = \frac{A'}{2} - j A' \pi - \frac{A'}{2} \qquad (2\text{-}10)$$

real and imaginary parts must be equal

$$d = - A' \pi \qquad (2\text{-}11)$$

$$A' = -\frac{d}{\pi} \qquad B' = \frac{d}{2\pi} \qquad (2\text{-}12)$$

Therefore the transformation relation is complete

$$z = \frac{d}{\pi} \left(\frac{1-w^2}{2} + \ln w \right) \qquad (2\text{-}13)$$

Now if the above equation could be solved for w, the problem would be much simplified. It would be necessary to find a harmonic function of w, invert the expression and plug into the expression for z, and then solve for the desired quantity.

For clarity, the following example is inserted.

Example

If the transformation had yielded

$$z = \pi d \, w^{1/2}, \qquad (2\text{-}14)$$

then

$$w = \left(\frac{z}{\pi d}\right)^2 \qquad (2\text{-}15)$$

A harmonic function of w is

$$\Omega = \frac{V_o}{\pi} \ln w \quad \text{(after some boundary conditions applied)} \qquad (2\text{-}16)$$

$$\Omega = \frac{V_o}{\pi} \ln\left(\frac{z}{\pi d}\right)^2 = \frac{2V_o}{\pi} \ln z - \ln(\pi d) \qquad (2\text{-}17)$$

$$z = r\, e^{i\theta} \qquad (2\text{-}18)$$

$$\Omega = \frac{2V_o}{\pi} \ln r + \frac{2V_o}{\pi} i\theta - \ln(\pi d) \quad \text{(complex potential)} \qquad (2\text{-}19)$$

The problem is then solved. Also there have been no approximations made. In continuing the first problem it was shown that for the stated geometry

$$z = \frac{d}{\pi}\left(\frac{1-w^2}{2} + \ln w\right) \qquad (2\text{-}13)$$

This is a transcendental equation. Therefore only an approximate solution is available. Now if we let w be expressed in polar coordinates

$$w = r\, e^{i\theta} \qquad (2\text{-}20)$$

the complex potential function is

$$\Omega = \Phi + j\Psi. \qquad (2\text{-}21)$$

A function which is harmonic will by definition satisfy Laplace's equation in polar coordinates. So if Ω is harmonic then:

$$\frac{\partial^2 \Omega}{\partial r^2} + \frac{1}{r}\frac{\partial \Omega}{\partial r} + \frac{1}{r^2}\frac{\partial^2 \Omega}{\partial \theta^2} = 0 \qquad (2\text{-}22)$$

The above is satisfied by

$$\Omega = A \ln \omega + B \qquad (2\text{-}23)$$

where A and B are arbitrary constants to be determined.

$$\Omega = A \ln (re^{i\theta}) + B \qquad (2\text{-}24)$$

$$\Omega = A \ln r + Ai\theta + B \qquad (2\text{-}25)$$

Now apply the boundary conditions to the complex potential (see Fig. 2(b))

$$\theta = 0 \quad \Omega = 0, \text{ and } \theta = \pi \quad \Omega = V_o \qquad (2\text{-}26)$$

$$0 = A \ln r + B \qquad (2\text{-}27)$$

$$V_o = A \ln r + Ai\pi + B \qquad (2\text{-}28)$$

$$V_o = Ai\pi \qquad (2\text{-}29)$$

$$A = \frac{V_o}{i\pi} \qquad (2\text{-}30)$$

Substituting (2-27) and (2-30) into (2-25) yields

$$\Omega = A \ln r + Ai\theta + B = \frac{V_o}{i\pi} i\theta \qquad (2\text{-}31)$$

$$\Omega = \frac{V_o}{\pi} \theta \quad \text{(complex potential)}. \qquad (2\text{-}32)$$

The charge $Q = \iint \vec{D} \cdot \vec{ds}$ \qquad (2\text{-}33)

The electric field E is

$$\vec{E} = - \nabla \Omega \qquad (2\text{-}34)$$

$$\vec{E} = - \frac{1}{r} \frac{\partial \Omega}{\partial \theta} a_\theta = - \frac{1}{r} \frac{V_o}{\pi} a_\theta \qquad (2\text{-}35)$$

$$E_N = - \frac{1}{r} \frac{V_o}{\pi} \qquad (2\text{-}36)$$

$$\iint \vec{D} \cdot \vec{ds} = \iiint \rho \, dv = Q \qquad (2\text{-}37)$$

$\epsilon E_N \, ds = - \rho \, ds$ (-ρ because the line integration of charge

density is over negative charge)

$$\rho = \frac{\epsilon}{\pi} \frac{V_o}{r} \qquad (2\text{-}38)$$

(See Fig. 2-1(b)).

$$Q = \int_{X_1}^{X_2} \left(\frac{\epsilon}{\pi} \frac{V_o}{r} \right) du$$

The charge per unit length is thus

$$Q(L) = \frac{\epsilon V_o}{\pi} (\ln X_2 - \ln X_1) \qquad (2\text{-}39)$$

$$z = \frac{d}{\pi} \left[\frac{1-w^2}{2} + \ln w \right] \qquad (2\text{-}13)$$

The point x=-ℓ in the z-plane maps to w=x_1 and w=x_2 in the w-plane because the mapping is conformal, and w has two values for each value of z because the plate in the z-plane has two sides of charge.

$$-\ell = \frac{d}{\pi} \left[\frac{1-X_1^2}{2} + \ln X_1 \right] \qquad (2\text{-}40)$$

$$-\ell = \frac{d}{\pi} \left[\frac{1-X_2^2}{2} + \ln X_2 \right] \qquad (2-41)$$

For $|\ell|$ ($|\ell|$ implies magnitude of ℓ) very large, $|X_1|$ is very small and $|X_2|$ is very large. Because we are trying to solve a transcendental equation the following approximations are made when $|\ell|$ is very large:

$$X_1 \text{ small}; \quad X_1^2 \text{ negligible} \rightarrow X_1^2 = 0 \qquad (2-42)$$

$$X_2 \text{ large} \rightarrow X_2^2 >> \ln X_2 \rightarrow \ln X_2 = 0 \qquad (2-43)$$

Substituting (2-42) and (2-43) into (2-40) and (2-41) respectively yields

$$-\ell = \frac{d}{\pi} \left[\frac{1}{2} + \ln X_1 \right] \qquad (2-44)$$

$$-\ell = \frac{d}{\pi} \left[\frac{1 - X_2^2}{2} \right] \qquad (2-45)$$

Solving for $\ln X_1$ in (2-44) yields

$$\ln X_1 = - \frac{\ell \pi}{d} - \frac{1}{2} \qquad (2-46)$$

Solving for $\ln X_2$ in (2-45) yields

$$\ln X_2 = \frac{1}{2} \ln \left[\frac{2\pi\ell}{d} + 1 \right] \qquad (2-47)$$

Substituting (2-46) and (2-47) into (2-39) gives

$$Q(L) = \frac{\varepsilon V_o}{\pi} \left[\ln X_2 - \ln X_1 \right] \qquad (2-48)$$

$$Q(L) = \frac{\varepsilon V_0}{\pi} \left\{ \frac{1}{2} \ln \left[\frac{2\pi\ell}{d} + 1 \right] + \left[\frac{\pi\ell}{d} + \frac{1}{2} \right] \right\} \qquad (2\text{-}49)$$

If we assume further that $\frac{\ell}{d} \gg 1$, then (2-49) will reduce to

$$Q(L) = \frac{\varepsilon V_0}{\pi} \left[\frac{1}{2} \ln \left(\frac{2\pi\ell}{d} \right) + \frac{\pi\ell}{d} \right] \qquad (2\text{-}50)$$

To compare the results with a crude approximation of an infinite parallel plate capacitor with no fringing fields we find that

$$Q = \frac{\varepsilon V_0 \ell}{d} \qquad \text{(charge per unit length} \qquad (2\text{-}51)$$
$$\text{on parallel plate capacitor)}$$

Subtracting (2-51) from (2-50) gives the charge due to the fringing capacitance, Q_f

$$Q_f = \frac{\varepsilon V_0}{2\pi} \ln \left(\frac{2\pi\ell}{d} \right) \qquad (2\text{-}52)$$

The total capacitance per unit length is thus the sum of the fringing and enclosed charge.

$$C = \frac{Q + Q_f}{V_0} = \frac{\varepsilon\ell}{d} + \frac{\varepsilon}{2\pi} \ln \left(\frac{2\pi\ell}{d} \right) \qquad (2\text{-}53)$$

For a transmission line the characteristic impedance per unit length is

$$z_0 = \frac{V}{I} = \frac{1}{uC} \qquad (2\text{-}54)$$

where u is the velocity of propagation of the wave along the line.

$$z_0 = \frac{1}{1/\sqrt{\mu\varepsilon} \, C} \quad \text{ohms} \qquad (2\text{-}55)$$

Using the capacitance calculated in Eq.(2-49) and assuming we now have two fringing fields, one on each side, the characteristic impedance of Eq.(2-55) becomes

$$Z_0 = \frac{\sqrt{\mu\epsilon}}{c} = (377) \frac{1}{\sqrt{\epsilon_r}} \frac{-1}{\frac{\ell}{d} + \frac{1}{\pi}[\ln(\frac{2\pi\ell}{d} + 1) + 1]}$$

(2-56)

This value of Z_0 is valid for ratios of ℓ/d greater than 3.0. A closer approximation for Z_0 valid for ℓ/d in the range 0.1 to 3.0 is

$$Z_0 = \frac{377}{\sqrt{\epsilon_r}(\frac{\ell}{d} + 1.0 + \frac{1}{\pi}\ln(\frac{2\pi\ell}{d} + 1))}$$

(2-57)

This equation is experimentally verified by the experimental data published by Hyltim [7] (see Fig. 2-6) and is compared with Eq.(2-59) and Wheeler's results in Table 2-2.

The effect of the dielectric filter is an important parameter to consider for dielectric constants different from 1. Wheeler [1] has solved this problem of finding the effective dielectric constant to be used.

$$\epsilon' = \frac{\epsilon + 1}{2} \cdot \left[1 + \left(\frac{\epsilon - 1}{\epsilon + 1}\right)\left(\frac{\ln \pi/2 + 1/\epsilon \ln (4/\pi)}{\ln (4\ell/d}\right)\right]$$

(2-58)

Table 1 has a few common dielectric constants and the value to be used for ϵ_r in equation (2-57) tabulated. In the case of microstrip the ratio of the width of the conductor (ℓ) and dielectric thickness (d) is also a variable which determines the effective dielectric constant ϵ'. It turns out that for a wide strip ($\ell \gg d$) above an infinite ground plane the characteristic impedance per unit length has been shown by Assadourian and Rimai [2] to be

TABLE 2-1

Dielectric Constant	Ratio ℓ/d	Effective Dielectric Constant
1	1	1.000
1	10	1.000
2	1	1.706
2	10	1.578
3	1	2.384
3	10	2.144
4	1	3.054
4	10	2.708
5	1	3.721
5	10	3.271
6	1	4.387
6	10	3.833
7	1	5.052
7	10	4.395
8	1	5.716
8	10	4.957
9	1	6.380
9	10	5.519
10	1	7.044
10	10	6.080
11	1	7.708
11	10	6.642

TABLE 2-2

CHARACTERISTIC IMPEDANCE

Ratio ℓ/d	Rimai [2] Eq.(2-59)	Wheeler [1]	Daniels Eq.(2-57)	Experimental (Hyltin)
0.1	491.089	373.417	300.352	299
0.2	420.151	330.886	258.384	250
0.3	367.591	297.650	230.263	227
0.4	327.061	270.898	209.447	206
0.5	294.835	248.859	193.101	190
0.6	268.586	230.359	179.754	176
0.7	246.780	214.588	168.552	168
0.8	228.370	200.968	158.955	160
0.9	212.614	189.076	150.600	151
1.0	198.971	178.954	143.235	145
2.0	122.486	116.200	98.432	107
3.0	89.337	86.903	76.143	85
4.0	70.651	69.679	62.430	70
5.0	58.593	58.274	53.044	60
6.0	50.138	50.139	46.180	
7.0	43.867	44.031	40.926	
8.0	39.021	39.271	36.769	
9.0	35.161	35.453	33.392	
10.0	32.010	32.320	30.593	

$$z_o = \frac{377}{\frac{\ell}{d} + \frac{2}{\pi} [\ln[1 + \frac{\ell}{2d}] + 1]} \quad \text{ohms} \qquad (2\text{-}59)$$

In the case of a narrow strip above an infinite ground plane $(d \gg \ell)$ the characteristic impedance was found to be

$$z_o = \frac{377}{2\pi} \cosh^{-1}(\frac{d}{\ell}) . \qquad (2\text{-}60)$$

Up until now, all formulation has been concerned with a single ribbon conductor on a dielectric over a ground plane. Now, let us look at a pair of conductors in what is called coupled microstrip. Judd et al. [3] have calculated the input impedance to a pair of coupled microstrip lines for two cases. When the currents in the lines are in phase (even mode) and when the currents are 180° out of phase (odd mode). Their results are displayed graphically in Fig. 2-2 with the parameters of line spacing and width over dielectric thickness to determine the characteristic impedance.

The above formulation has all been concerned with microstrip. Strip-line or sandwiching the center slab line between two ground planes gives the transmission system a built-in shielding. Work has been done by Cohn [4] for the case of coupled strip line. He has shown that for the case of even mode symmetry the characteristic impedance is

$$z_{oe} = \frac{30\pi}{\sqrt{\epsilon_r}} \cdot \frac{K(k_e')}{K(k_e)} \ \Omega \qquad (2\text{-}61)$$

where $k(k_e)$ is the elliptic integral of the first kind and
$k_e = \tanh(\frac{\pi}{2} \cdot \frac{\ell}{d}) \cdot \tanh(\frac{\pi}{2} \cdot \frac{\ell+s}{d})$ and $k_e' = \sqrt{1 - k_e^2}$.
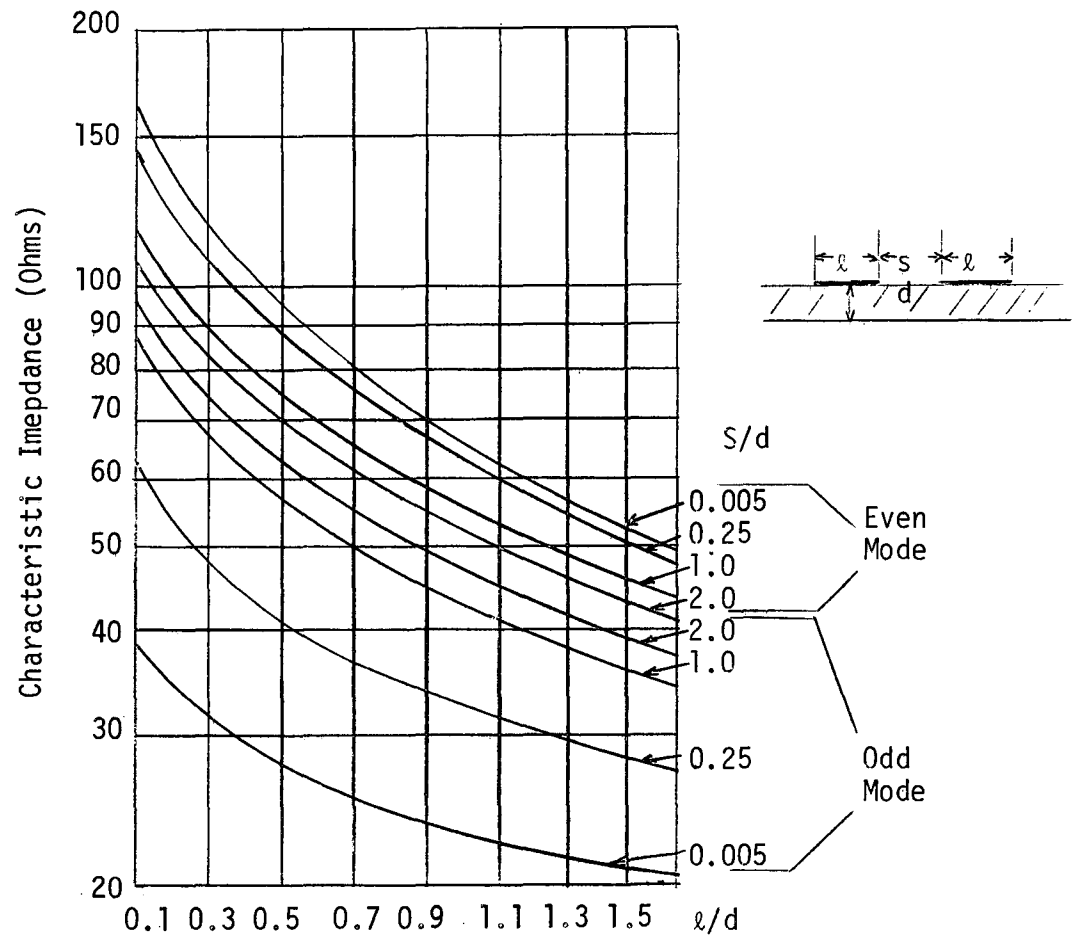
Fig. 2-2. Even- and odd-mode impedances for parallel-coupled microstrip transmission lines (ε_r = 9.5).

For the case of odd mode symmetry

$$k_o = \tanh \left(\frac{\pi}{2} \cdot \frac{\ell}{d}\right) \cdot \coth \left(\frac{\pi}{2} \cdot \frac{\ell+s}{d}\right) . \qquad (2\text{-}62)$$

Because the elliptic integral is a tabulated function, graphs of solution are possible.

Hilberg [5], following a similar manner, has computed even and odd mode z_o and his results compare almost identically with those of
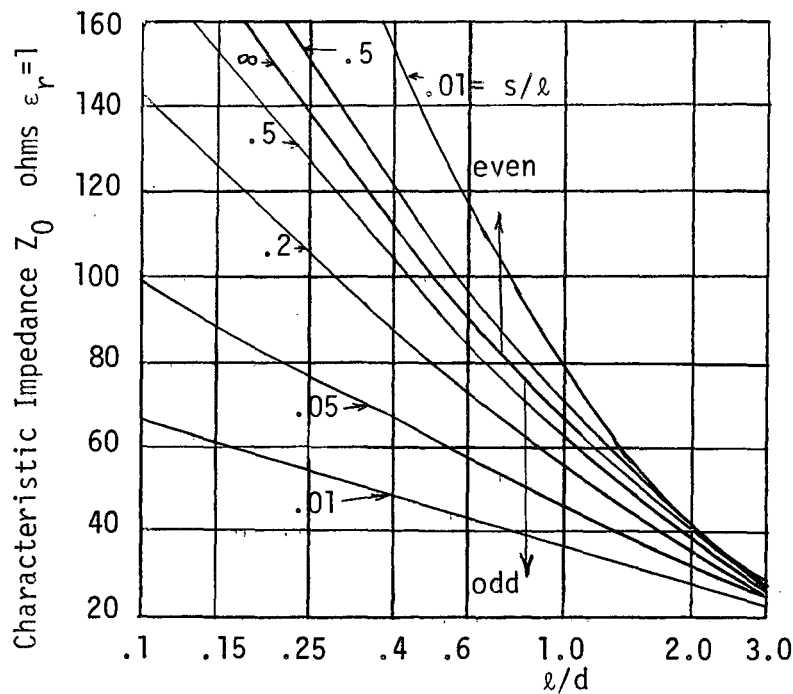
Fig. 2-3.   Even- and odd-mode impedances for
             parallel-coupled stripline.

Cohn.   Hilberg's results, however, include a wide range of values for

ℓ/d ranging up to 100 and down to 1/1000.   Hilberg's generating

functions are

$$Z_{odd} = \frac{\eta}{2\pi} \ln \left[\frac{2 \sqrt{\sinh \frac{\pi u_2}{h} / \sinh \frac{\pi u_1}{h}} + 1}{\sqrt{\sinh \frac{\pi u_2}{h} / \sinh \frac{\pi u_1}{h}} - 1} \right] \qquad (2-63)$$
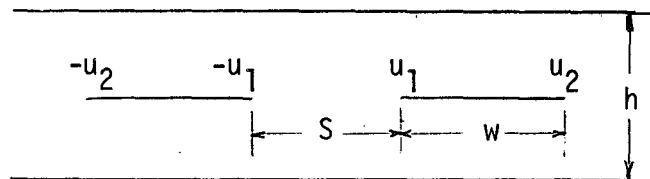
Fig. 2-4.   Geometry for Eq. 2-63.

To determine Z_{even} replace all sinh(x) by cosh(x) in Z_{odd}.
Cohn also included a very useful nomogram from which design of a stripline can be made for a desired z_o.

Bates [6] used conformal mapping to determine the characteristic impedance of a shielded slab line but he took it one step further by considering the thickness of the line. His results are in the form of a useful design graph. (See Fig. 2-5).

In the case of microstrip on semiconductor (Si) Hyltin [7] conducted experimental verification of calculated values of Z_o for ε_r = 11.7. He compared his results with Assadourian and Rimai and there is a definite difference, however when compared with my results his experimental and my theoretical results are extremely close.
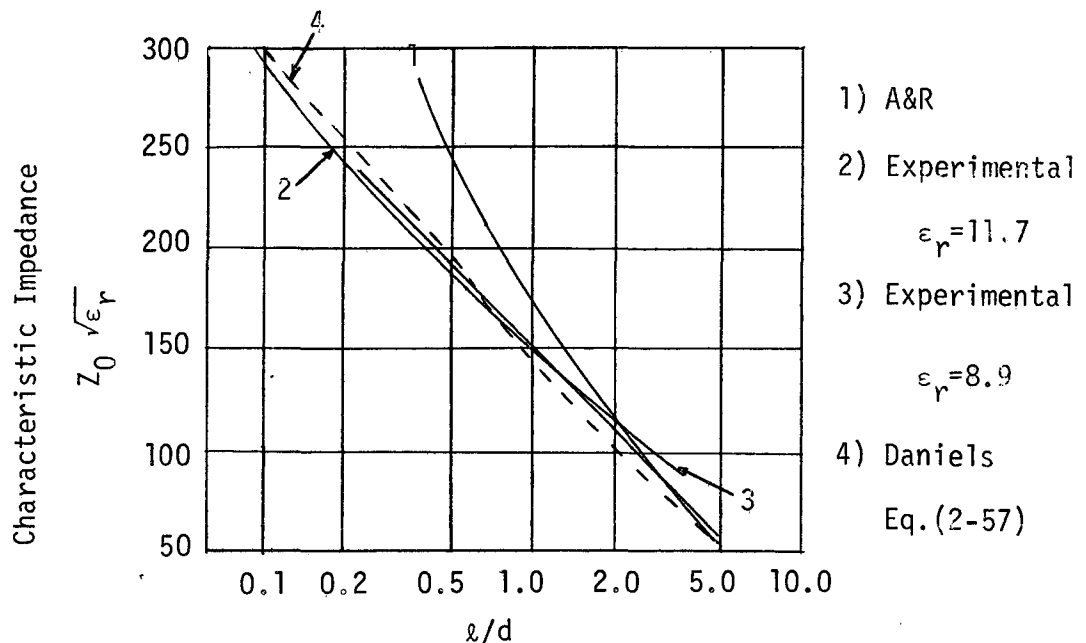
Fig. 2-6. Characteristic impedance of microstrip with experimental vs. theoretical curves.

c
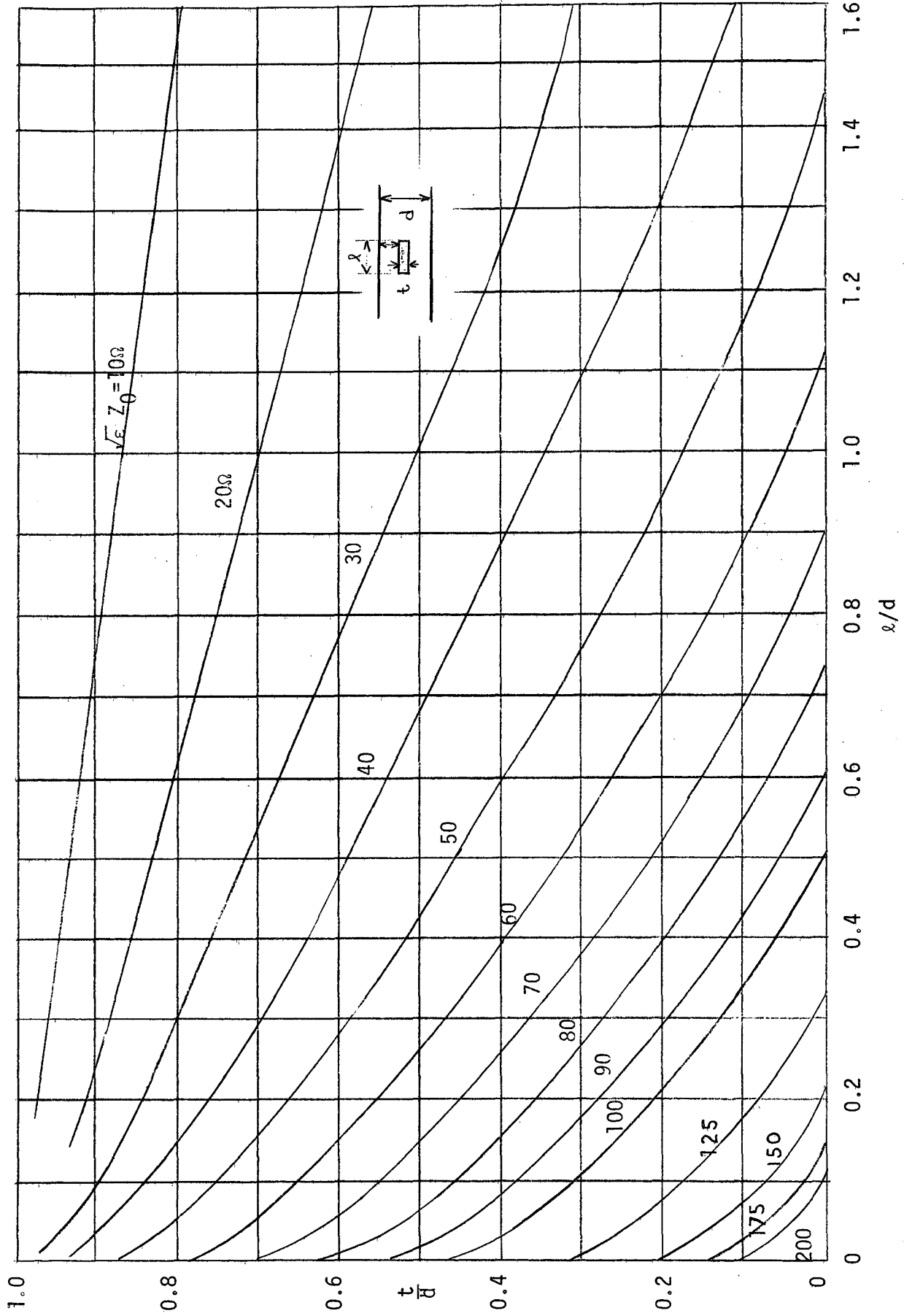
Fig. 2-5. Stripline characteristic impedance with thickness of conductor as a parameter.

B.   ITERATION TECHNIQUES

The important concept to realize here is that many different types of complicated geometries can be solved quickly by this method on a digital computer. The theory behind the program is that a Taylor series expansion can be made of the potential function about a point.

$$V(x) = V(a) + (x - a) \left.\frac{\partial V(x)}{\partial x}\right/_{x=a} + \frac{(x-a)^2}{2!} \left.\frac{\partial^2 V(x)}{\partial x^2}\right/_{x=a} + \ldots \qquad (2\text{-}64)$$

It should be noticed if the expansion about a = 0 of V(x) in the +X direction is added to a similar expansion in the negative x direction, the result will yield a term $\partial^2 V/\partial x^2$. If the same technique is used in y directions $\partial^2 V/\partial y^2$ will be obtained. The sum of these will yield Laplace's equation which must equal zero in the charge free region. Of course, appropriate approximations must be made. A conditional result is that the distance between the test points must be small compared with the geometry.

For every point an equation will result. Thus the problem is to solve a number of simultaneous equations. Green [8] used a method known as successive over relaxation to solve these equations. Use of the equation

$$V_i (j+1) = V_i (j) - \frac{\Omega}{a_{ij}} \sum_{k=1}^{n} a_{ik} V_k (j) - b_i \qquad (2\text{-}65)$$

where $AV = B$

a_{ik}, v_i, b_i terms of matrices A,V,B

j = number of iteration cycles

n = number of simultaneous equations

Ω = accelerating factor (best Ω = 1.95)

This method yields values corresponding to one set of input data as opposed to the functional equations yielded by conformal mapping. Green's results published in the form of a graph (see figure) compares favorably with my analytic results.
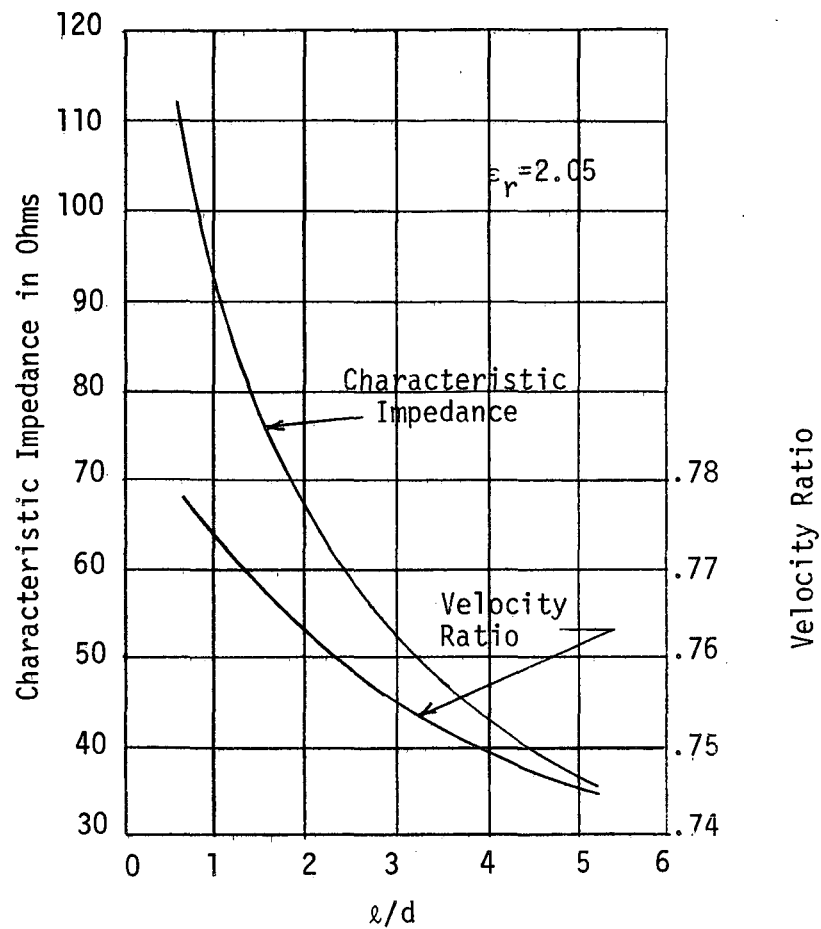
Fig. 2-7. Microstrip characteristic impedance
solved using Greens method.

C. VARIATIONAL METHOD

The solution of Poisson's equation

$$\nabla^2 \phi = -\frac{\rho(x,y)}{\varepsilon} \tag{2-66}$$

when inserted into

$$\frac{1}{C_0} = \frac{1}{Q^2} \int_S \rho(x,y) \, \phi(x,y) \, dS \tag{2-67}$$

gives the capacitance of the geometry whose boundary conditions were used to solve the differential equation. For the case of the infinitely thin strip the charge density may be expressed as

$$\rho(x,y) = f(x) \, \delta(y-b) \, . \tag{2-68}$$

If the Fourier transformation of ϕ and f are taken and inserted into the function of capacitance

$$\frac{1}{C_0} = \frac{1}{2\pi Q^2} \int_{-\infty}^{\infty} \tilde{f}(\beta) \, \tilde{\Phi}(\rho,h) \, d\beta \tag{2-69}$$

If this expression can be evaluated, the characteristic impedance can be determined from

$$z_0 = \frac{377}{C_0 \sqrt{\varepsilon_r}} \varepsilon \tag{2-70}$$

Yamashita and Mittra [9] evaluated this expression for capacitance on a digital computer. They used for $f(x)$

$$f(x) = |x| \tag{2-71}$$

x in the range of the strip width.

Their results are displayed graphically and compare with my
results and Wheeler's results favorably. They also have graphical
data for the cases of finite thick slab above ground plane.
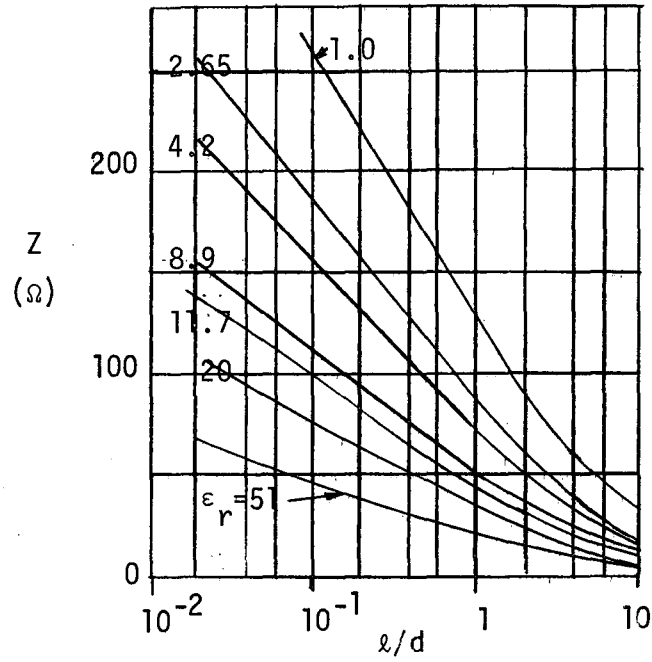
Fig. 2-8. Characteristic impedance for various dielectric
constants of microstrip.

CHAPTER III

MICROWAVE INTEGRATED-CIRCUIT TECHNOLOGY

In this chapter some of the basic design and fabrication methods
applicable to microwave integrated circuits are discussed. Some good
survey papers [11,18,19] exist on the topic, and these are referenced
freely. Presently elements for microwave circuits are categorized as
either lumped or distributed. With lumped elements, performance is
independent of frequency over the range of interest while distributed-
circuit elements must be treated with transmission line techniques
and have element values which are sensitive to frequency and line-
length variations.

Lumped elements are physically small compared to a wavelength, and
as long as this constraint can be met, it is possible to obtain element
values which are independent of frequency and behave pretty much as
their low frequency counterparts. Lumped circuits are flexible in that
they can be designed so that element values can be changed after the
device has been fabricated, a feature not so easily accomplished with
microstrip circuits. Lumped elements are amenable to batch processing
and with present technology and fabrication procedures are practical
through 12 GHz and feasible to even higher frequencies (20 GHz).
According to Caulton et al.[19] they are currently very competitive
with microstrip through 6 GHz from cost, size, and design complexity

considerations as evidenced by the following commercial lumped element devices:

(1) S band amplifiers (expecially suited for high power designs) 6 watts cw, 26% efficient, 35 db gain, 2.25 GHz transistor amplifier.

(2) C-band impedance transformers built and tested

(3) Filters and quadrature hybrids.

As element size becomes an appreciable fraction of a wavelength, lumped devices look more and more distributed. This and the increase in parasitic effects with frequency set the upper frequency limits for lumped elements. It has been reported [19] that single turn inductors remain truly "lumped" to about 12 GHz. Multiturn spiral inductors which have potentially higher Q's than single turn inductors begin to suffer from interturn capacities and distributed effects earlier and their usefulness is limited to about 6 GHz. Also because of the interturn capacities, the maximum achieveable resonant frequencies for multiturn spiral geometries are lower than for single turn. Using thin film technqiues lumped capacitors having Q's from 600 to 5000 can be constructed with values typically ranging from 0.1 to 50 pf. Capacitors easily remain "lumped" for frequencies up to 12 GHz.

Distributed circuit element realizations at microwave frequencies are possible using microstrip, slot line, coplanar waveguide, and stripline. Microstrip will be emphasized in this discussion because of its widespread adoption by users. It consists of ribbon conductors separated by a dielectric substrate from a conducting ground plane . The fields propagate with a quasi-TEM mode, and a detailed analysis

of their behavior is given in Chapter II. Two additional ways of
realizing distributed circuit performance, slot line [20] and coplanar
waveguide line [21], are shown respectively in Figs. 3-1 and 3-2.
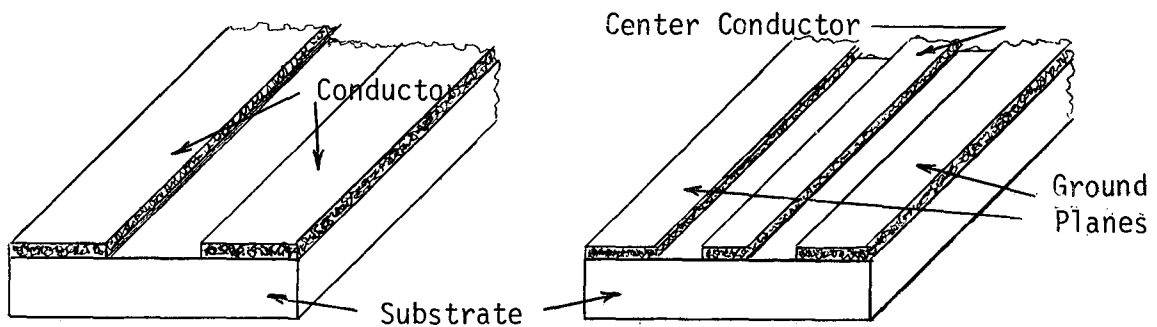
Fig. 3-1. Slot Line Construction.   Fig. 3-2. Coplanar Wave-
                                                 guide Construction.

Both have the advantage of allowing shunt mounting of devices without
the need for drilling holes in the substrate, but neither are widely
used yet.

A. LUMPED ELEMENT DESIGN

For an element to be truly lumped its electrical length must be
much smaller than a wavelength or the element would introduce a
terminal-to-terminal phase difference. Therefore, it is obvious that
when the operating frequency is Ku band (12-18 GHz) the lumped circuit
elements are extremely small. The development of photolithographic
technology has made it possible to fabricate these small circuits
inexpensively and reliably. Because the operating frequencies are so
high the values which must be realized are small, for example an
inductor of a few nanohenrys is all that is required.

In the case of a capacitor, 50 picofarads is a large value and even this is easily realized. The formulas to compute the values of these lumped elements are classical and are approximate, but they yield values which are close enough. The formula for a ribbon inductor (see Fig. 3-3) is [10]:

$$L = 5.08 \times 10^{-3}\ell \ [\ln \frac{\ell}{w+t} + 1.19 + 0.22 \frac{w+t}{\ell}]$$ (3-1)

where

L = inductance in nanohenrys

w = width of inductor in mils

ℓ = length of inductor in mils

t = thickness of inductor in mils
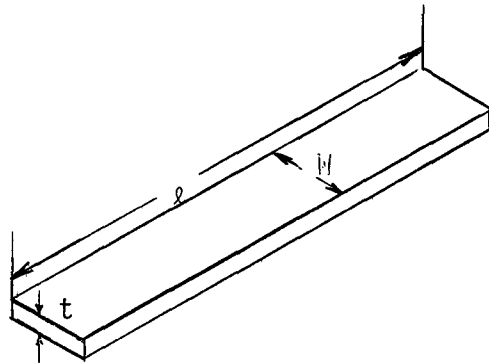
Fig. 3-3. Ribbon Inductor in Free Space.

The ratio of the stored energy to the average power loss in an element is called the quality factor, Q. The unloaded Q of the ribbon inductor is

$$Q = \frac{wL}{R}$$ (3-2)

where R is the high frequency resistance of the ribbon and is expressed as

$$R = \frac{KR_s \ell}{2(w+t)} \qquad (3-3)$$

K is the correction factor and is plotted vs. w/t in Fig. 3-4 and R_s
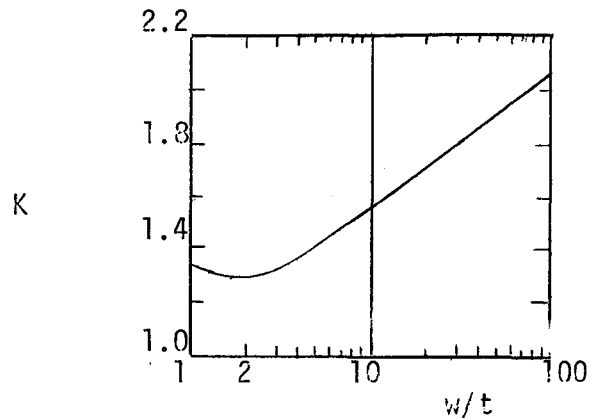
Fig. 3-4. Correction Factor K as a Function of w/t.

is the sheet resistance in ohms. For copper, R_s is $2.61 \times 10^{-7}\ f^{1/2}$ (see Table 3-1). In order to obtain higher inductive values while conserving chip area it is standard to use a spiral ribbon inductor (see Fig. 3-5). Because of mutual coupling, the formula for computing the values is [10]:

$$L = \frac{n^2 (d_o + d_i)^2}{32(d_o+d_i) + 88(d_o-d_i)}\ \text{nanohenrys} \qquad (3-4)$$

where

n = number of turns

d_o = outer diameter in mils

d_i = inner diameter in mils.
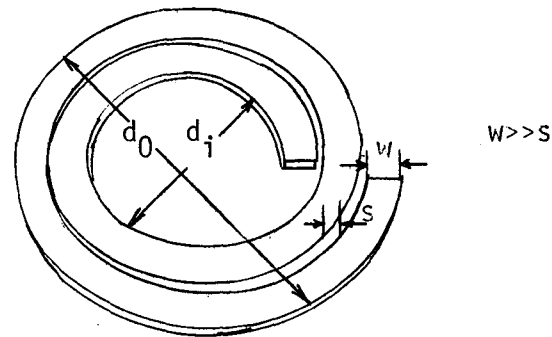
Fig. 3-5. Lumped Spiral Inductor.

The Q of the spiral inductor is

$$Q = \frac{8f \ Lw}{K'R_s \ n(d_o + d_i)} \qquad (3-5)$$

There exists an optimum value for the ratio of d_o to d_i, and it turns out that for $d_o = 5 \ d_i$, the Q of the spiral inductor is highest. There must be some space, d_i, to allow lines of flux to pass through the center in order to increase the stored energy per unit length. Also the spiral arms should be kept as wide as possible with the space between the arms kept large enough to avoid parasitic distributed capacitances. The use of a square coil increases the inductance per unit area, but its Q is less than that of a spiral inductor. In the case that the inductor is above a ground plane the ratio of dielectric thickness to conductor width should be greater than 20 [11] in order to avoid parasitic effects.

The lumped element capacitor is realized by the classical metal-dielectric-metal sandwich and its value, neglecting fringing fields, is given by

$$C = \frac{\varepsilon S}{d} \qquad (3\text{-}6)$$

$\varepsilon \;=\; \varepsilon_r \varepsilon_o$

$\varepsilon_r \;=\;$ relative dielectric constant

$\varepsilon_o \;=\; 5.7 \times 10^{-11}$ farads/cm

S $\;=\;$ surface area of the top metal (ℓ x w)

d $\;=\;$ distance separating the top metal from the ground plane.
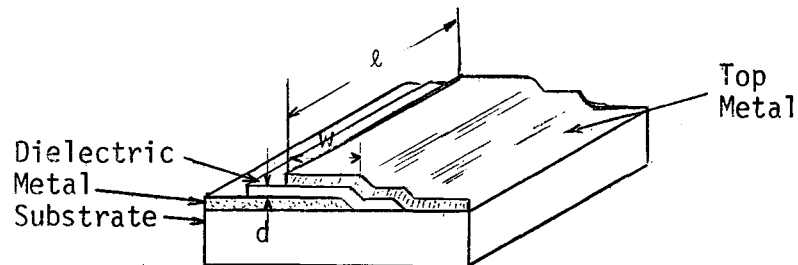
Fig. 3-6. Lumped Element Capacitor.

The Q of the capacitor where S is square (ℓ = w) is given by

$$Q = \frac{Q_c \, Q_d}{Q_c + Q_d} \qquad (3\text{-}7)$$

where

$$Q_c = \frac{3}{2\omega \, R_s \, C} \qquad (3\text{-}8)$$

$$Q_d = \frac{1}{\tan \theta} = \frac{2\pi f \varepsilon}{\sigma} \quad \begin{array}{l}(\tan \theta \text{ is the} \\ \text{dielectric loss tangent})\end{array} \quad (3\text{-}9)$$

The microwave lumped resistor is obtained by depositing a thin film of metal where its value is the sheet resistance of the metal. However, the input impedance to this resistor must take into account the capacitive value of the metal film. Thus the impedance of this resistor where $R_s \gg \omega L$ is:

$$Z_{in} = \frac{R_s}{\frac{w}{\ell} + j \frac{\omega C R_s}{3}} \quad (3\text{-}10)$$

In all the cases of lumped elements the metal film thickness should be at least 3 skin depths where the skin depth, δ, is given by

$$\delta = \frac{1}{\sqrt{\pi f \mu \sigma}} \quad (3\text{-}11)$$

μ = permeability of metal

σ = conductivity of metal

f = frequency of operation.

B. DISTRIBUTED ELEMENT DESIGN (Microstrip)

Microstrip circuit design is a distributed element approach and probably has the edge over lumped elements for Ku-band and above with present fabrication technology. Microstrip is an unbalanced transmission-line structure which is constructed as shown in Fig. 3-7. A high dielectric constant substrate is coated on one side with a ground plane conductor, and a ribbon conductor whose width and height above

the ground plane for a fixed substrate dielectric constant can be varied to control line characteristic impedance. The electromagnetic
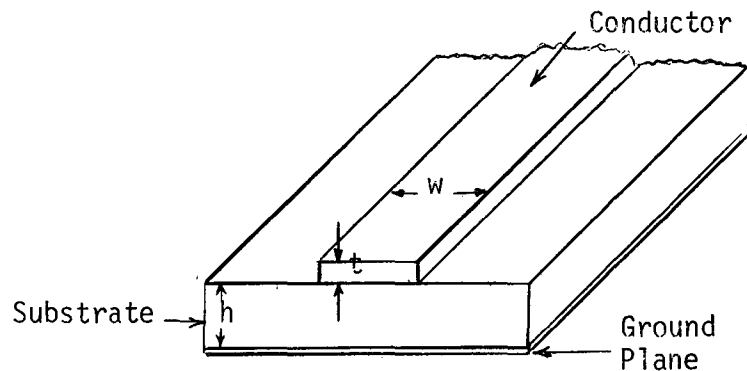
Fig. 3-7. Microstrip Transmission-Line.

propagation along the microstrip circuit is quasi-TEM with fringe fields extending beyond the conductors. This changes the dielectric constant of the substrate to some effective value, a trade off between air and the substrate (see Table 2-1). For this reason, the packages are not as small as you would expect and in all cases are much larger than lumped element design. However, distributed-element design has a better reproducability than lumped element. The distributed-element network parameters are per unit length with the usual quantized transmission-line model shown in Fig. 3-8.

D
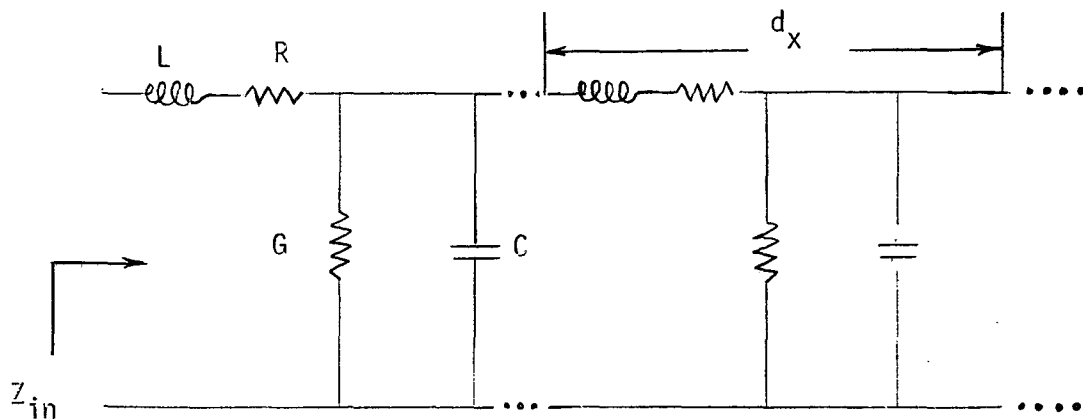
Fig. 3-8. Transmission Line with Series-Inductance L and Resistance R per Unit Length, and Shunt-capacitance C and Conductance G per Unit Length.

In order to adjust complex impedance values, the line lengths can be varied. At a fixed frequency, the value for the input impedance to a distributed transmission line system is given by the transformation:

$$Z_{in} = Z_0 \frac{Z_L + j Z_0 \tan \beta L}{Z_0 + j Z_L \tan \beta L} \qquad (3-12)$$

where:

Z_0 = characteristic impedance of the line (Eq. 2-57)

Z_L = load impedance

β = $2\pi/\lambda$ (λ = wavelength on line)

L = length of line.

To realize shunt inductors and capacitors with distributed elements, open and short circuited stubs are commonly used. When microstrip is used, the circuit losses present will be due to dielectric and conductor losses and the surface roughness of the substrate. Dielectric loss is given by [12]

$$\alpha_d = \frac{q\pi}{\lambda_o} \frac{\varepsilon_r}{\sqrt{\varepsilon_r'}} \tan \Psi \qquad (3\text{-}13)$$

α_d = dielectric loss in nepers per unit length

q = filling fraction (see Fig. 3-9) [1]

ε_r = relative dielectric constant of the substrate

ε_r' = effective dielectric constant (Table 1-1)

$\tan \Psi$ = dissipation factor of substrate (typical value for Al_2O_3 is 0.0001 @ 10 GHz)

λ_o = free space wavelength
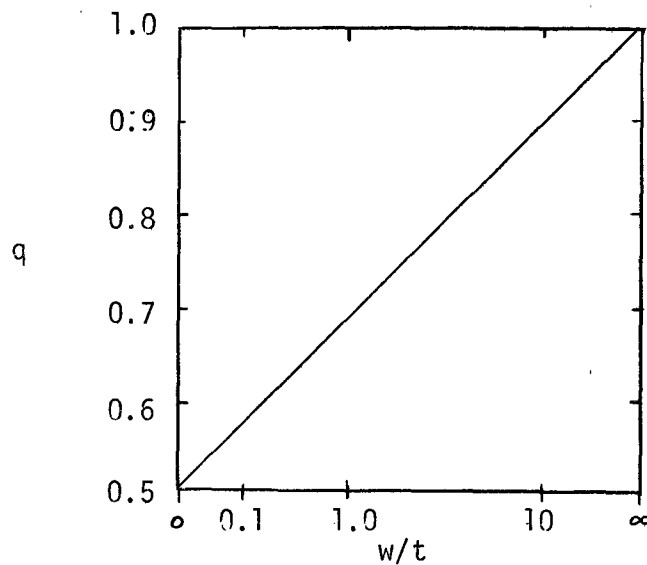
Fig. 3-9. Filling Fraction of Microstrip vs. Strip Width over Substrate Thickness

The conductor losses can be found using:

$$\alpha_c = \frac{62.8}{Z_o w} \sqrt{f\rho} \qquad (3\text{-}14)$$

Z_o = characteristic impedance of microstrip (Eq. 2-57)

w = width of the conductor

f = frequency in GHz

ρ = resistivity of the conductor

When evaluating the losses due to surface roughness just consider that smoother surface finishes have lower losses. Production technology is the limit to minimizing this loss factor.

C.   PRODUCTION TECHNIQUES

In order that the losses due to surface roughness be minimized, it is necessary to polish the substrate surface to a fine degree (2 microns or better). There are two ways metal can adhere to the substrates, by mechanical bond or chemical bond. For there to be a mechanical bond the surface is necessarily rough, so chemical bonds are required from a loss consideration in MIC devices. Experimental evidence indicates that the best procedure in making a chemical bond is to evaporate a layer of chrome 50-400 Å thick or another reducing material onto the surface of the heated substrate and allow a chrome-oxide bond to form. Then another layer of pure chrome is evaporated and any good metal will adhere to this outer layer of pure chrome.

Typical Thicknesses
5μm
.1μm
50 Å

conductor metal
chrome
chrome oxide bond
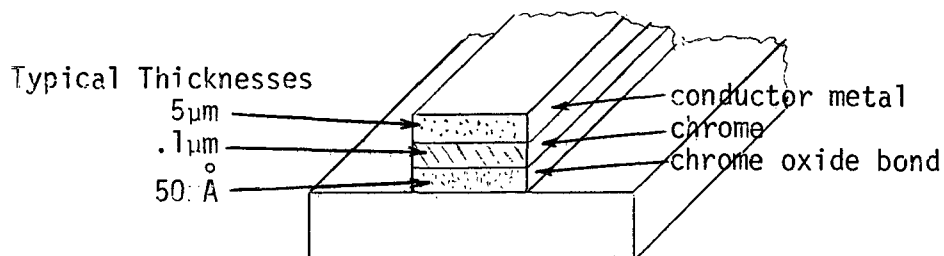
Fig. 3-10.   Layers of Metal in a Chemical Bond.

A very good combination of metals is the chrome-silver-gold chemical bond.
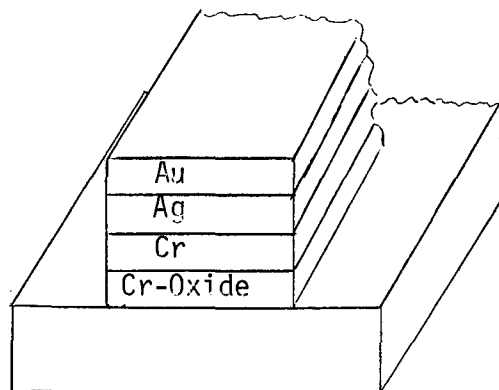
Fig. 3-11. Layers of a Chrome-Silver-Gold Metalization.

In Cr - Ag - Au metalization chrome which adheres to the substrate is initially applied. The intermediate vaporization of silver is used to separate the gold from the chrome preventing the occurrence of Cr - Au intermetallic solid solutions which are difficult to etch and also the Cr - Au combination at high temperatures causes an increase in resistivity resulting in a loss in RF power. The gold outer layer is employed as a nonoxidizable bonding surface. The Ag-Au layers which make up the current carrying portion of the metalization system have greater atomic masses, greater activation energies for self-diffusion, and higher melting points than does aluminum. Obviously, the gold system is preferred to other metalization schemes for application where a higher current carrying and thus power handling capability is desired. If aluminum were used, the current density would be limited to less than 10^6 amperes/cm^2 at elevated temperatures due to electromigration.

There are several other metal combinations which can be used effectively such as:

Cr - Cu - Au

Cr - Cu

Cr - Cu - Ni - Au

Ti - Pd - Au

Ti - Pt - Au

Ta - Au

Tantalum or Titanium can be used as an alternate adhesion layer while copper is an alternate surface layer. Copper is binded using soldering techniques. The bulk characteristics of a few conductors are given in Table 3-1 [18].

Table 3-1
PROPERTIES OF METALS FOR MIC APPLICATIONS

Material	Melting Point °C	Skin Depth (μm) @ 2 GHz	Surface Resistivity $\Omega/sq. \times 10^{-7} \sqrt{f}$	Coefficient of Thermal Expansion $\alpha_T/ C \times 10^{-6}$	Adherence to Film or Substrate
Ag	961	1.4	2.5	21	Poor
Cu	1084	1.5	2.6	18	Very poor
Au	1063	1.7	3.0	15	Very poor
Al	660	1.9	3.3	26	Very poor
Cr	1860	2.7	4.7	9	Good
Ta	2980	4.0	7.2	6.6	Good
Ti	1670	10.5	16.1	8.5	Good

The metalization system best suited to the job should be chosen considering:

    (1) Passive elements required

    (2) Environmental and processing temperatures

    (3) Compatibility with active devices.

Tantalum has been used effectively to realize capacitors, resistors and interconnections. Tantalum's high melting point makes it desirable for realizing high power elements. Tantalum also offers the property that it can be anodized to form dielectric films. When sputtered on to the substrate it forms resistive films. The properties of other dielectric and resistive films are given in Tables 3-2 and 3-3 respectively [18].

Table 3-2

DIELECTRIC FILM PROPERTIES

Material	Relative Dielectric Constant, ε_r	Dielectric Strength V/CM	Microwave Q
SiO_2 (evaporated)	6-8	4×10^5	30
SiO_2 (deposited)	4	10^7	20-5000
Al_2O_3 (anodized or evaporated)	7-10	4×10^6	
Ta_2O_5 (anodized or sputtered)	22-25	6×10^6	< 100

Table 3-3

RESISTIVE FILM PROPERTIES

Material	Resistivity Ω/square	Low Temperature Coefficient of Resistivity $(^\circ/_\circ/^\circ C)$	Stability
Cr (evaporated)	10-1000	-0.1 to +0.1	Poor
NiCr (evaporated)	40-400	+0.0002 to +0.1	Good
Ta (sputtered in anodized-nitride)	5-100	-0.01 to +0.01	Excellent
Cr-SiO (evaporated or cermet)	to 600	-0.005 to -0.02	Fair
Ti (evaporated)	5-2000	-0.1 to +0.1	Fair

A good substrate should have the following general properties:

(1) low loss for the operating frequency

(2) chemical adherence for conductors

(3) smooth surface

(4) retain above during processing

(5) amenable to cutting and drilling.

Some of the commonly used substrates along with their x-band characteristics are listed in Table 3-4.

Table 3-4

PROPERTIES OF SUBSTRATES

Material	Loss Tangent @ 10 GHz x 10^4	ε_r	Thermal Conductivity (watts/cm °C)
Alumina	2	9.6-9.9	0.2
Sapphire	< 1	9.3-11.7	0.4
Glass	> 20	5	0.01
Beryllium oxide	1	6	2.5
Rutile	4	100	0.02
Ferrite/garnet	2	13-16	0.03
Galium arsenide	16	13	0.3

Presently there are two ways geometrical metal shapes can be put on the substrate or oxide top layer, thin and thick film processing. The terms "thick" and "thin" date back to low frequency applications, and it must be kept in mind that they do not necessarily indicate the actual metal thickness but only the way in which the metal is deposited. Both processes can be used to obtain the 3-5 skin depth thickness of metal needed for microwave circuits. The several techniques of "thin" film fabrication are:

    (1)   Vacuum deposition (10^{-7} torr, electron beam vaporization of metal to be used)

    (2)   Sputtering (10^{-2} torr, filament of metal to be deposited)

    (3)   Anodization (plating)

    (4)   Ion beam deposition.

This process has a much lower dc resistance than the thick film results,

and hence it is greatly preferred for precision, low loss applications. "Thick" film processing includes:

(1) Screening and firing (similar to graphics)

    (a) silk screening

    (b) steel mesh screening

(2) Pyrolytic

    (a) vapor anodization

    (b) glass deposition

Thick film processing is less costly than thin film and requires less sophisticated equipment. But as stated the bulk properties of the conductors are the trade off for low cost.

Plating-etching and etching thick metal are two thin film processes used today. The former should be used when a high degree of line resolution is desired, while the latter method has conductors which exhibit better bulk properties. In the plating-etching technique a thick layer of photoresist is deposited on top of the evaporated seed metal (Cr-Ag). The photoresist is then exposed under the high resolution plates and developed. Thus a trench (see Fig. 3-12(a)) is left in the photoresist which will be filled by anodizing or plating.

Photoresist

Seed Metal

$\left(\begin{array}{c} 1\,\mu m \\ Cr\text{-}Ag \end{array} \right)$

Trench

Substrate

Au   Cr-Ag

Substrate

(a) before plating   (b) after deposition - etching
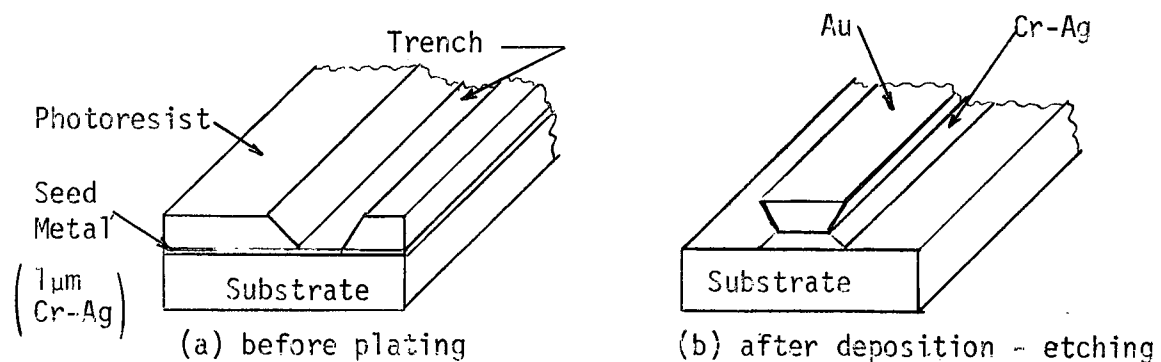
Fig. 3-12. Plating-etching Process.

After the metalization (plating) the excess photoresist and metal are etched away.

In the etching thick metal process, a thin layer of photoresist is spun onto the completely plated substrate and photolithographically processed. The substrate is then put into an etching solution which etches away all the metal not under the protective photoresist. (See Fig. 3-13).
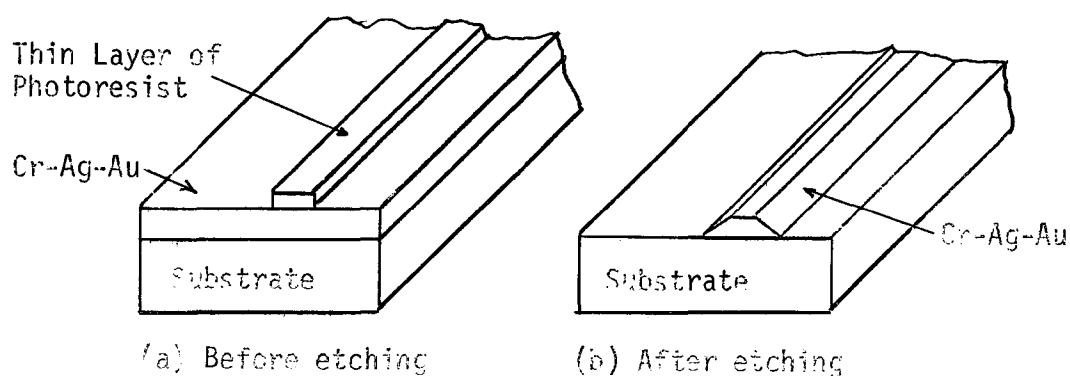
Fig. 3-13. Etching Thick Metal Process.

In the plating etching procedure only the 1 μm thick seed metal is subject to undercut, thus allowing 5 μm or greater line resolution. When the etching thick metal process is used, an undercut of twice the thickness of the photoresist line is left. At lower microwave frequencies microstrip line widths are great, and a high degree of line resolution is not required. Thus, the simpler method of etching thick metal with its good bulk properties would be suited to microstrip.

The methods by which these circuits are realized are classified as either hybrid or monolithic. In the hybrid technique the active devices are mechanically mounted on the substrates which contain the lumped elements and feeds. The monolithic approach would be the most ideal if high resistive semiconductor substrates could stand processing and not loose their resistivity. Here the active devices would be grown epitaxially in pockets in the insulating substrate. A trade off between the two aforementioned cases could be termed quasi-monolithic and consist of depositing silicon on alumina and then processing. Silicon-on-sapphire, SOS, techniques are still being investigated to solve material faults and crystal orientation problems.

CHAPTER IV

ARRAY IMPEDANCE MATCHING

This chapter deals with the theory and methods of wide angle impedance matching a nonuniform antenna input impedance. The possibility of using microstrip techniques to incorporate behind-the-array matching circuitry directly into modular-array elements will be investigated. The theory to be used is set forth by Hannan et al. [13]. In their example a phased array antenna element is treated as a nonlinear one port network. Mutual coupling above the array surface causes array element driving point impedance to change with scan angle and Hannan et al. showed that the effect can be compensated beneath the array surface with interconnecting circuits. Discussion of the realization and construction of these match-ing circuits using MIC (microwave integrated circuit) techniques is included in this chapter. A sample compensation is worked out based on experimental data for an array of $\lambda/2$ dipoles without compensation whose input impedance variations due to scan angle were found in the literature. In Hannan's method a shunt admittance between two adjacent array elements results in an equivalent phase dependent shunt to ground for each element. The magnitude of the equivalent admittance is proportional to $\sin^2(\delta/2)$ where δ is the phase increment between elements, and this property is used to obtain wide angle matching. Some alternate WAIM compensation techniques are baffles, fences, and dielectric cover sheets. These are compared Table 4-1. The baffles and fences are

electrical obstructions introduced between elements on the array surface to diminish mutual coupling between array elements. These obstructions alter the fields about the antenna such that a single element's pattern will be less than ideal and also cause shadowing which limits the extent of wide angle scans. Recall that the ideal array element for wide scan cones is one which is hemispherically isotropic. On the other hand, dielectric cover sheets do not appreciably affect the antenna pattern.

A plane EM wave incident on a dielectric sheet sees an effective wave impedance at the interface with the dielectric. This impedance is a function of the angle of incidence of the wave. Thus a compensating impedance which varies with scan angle can be obtained if a properly dimensioned dielectric slab is placed in the array environment as seen in Fig. 4-1. Tappered thicknesses of dielectrics and non-uniform permittivities might be used to effect WAIM for finite arrays much the same way behind the array coupling is used.
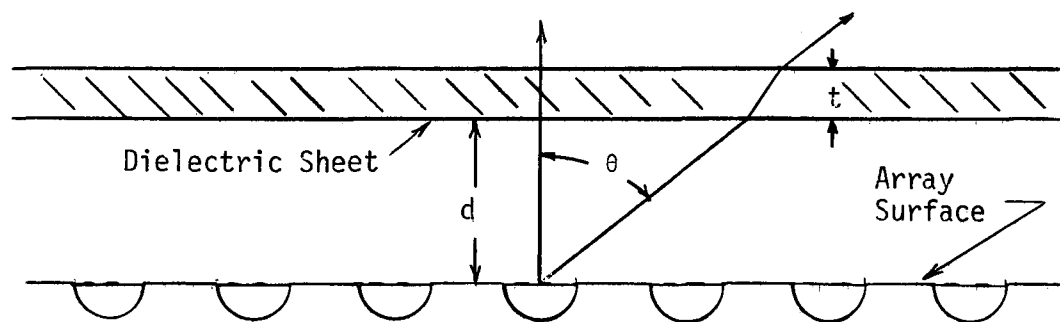

Fig. 4-1. Dielectric Cover Sheet a Distance d Above Array Surface

Matching Technique	Behind the Array Lumped	Distributed	Dielectric Cover Sheet Uniform	Non-Uniform	Baffles-Fences
Cost Units	3-4	3-5	1-2	3-5	1
Applicable Frequency Range	L,S,X Bands	L,S,X,K_u Bands	L,S,X,K_u Bands		L,S,X Bands
Array Surface Restrictions	not acceptable		Environmental Dependence of Dielectric		Aerodynamically Limited
Degree of Compensation Attainable	Precise, any Value	Band Limited	Good		Fair, also limits max. scan angle
Fabrication Difficulty Units	3-4 to X Band	3 to K_u Band	1	4	4-5
Power Consumption	Many Losses		Medium		Low

Table 4-1. Comparison of Compensation Techniques

Any of the above methods could be used in tandum, but this is not recommended from a cost and complexity consideration. As far as efficiency versus cost the most applicable means amoung the individual WAIM techniques for matching would seem to be the dielectric sheet. In this chapter, the method of interconnecting circuits is explored in detail and an example is worked out in terms of component values. The results show that the Hannan method is feasible, however, it presently is not cost and design time competitive. In future applications the Hannan scheme may still find use in active element or high frequency arrays. In order to obtain a low cost array of active elements for instance, mass production is inevitable and modular "integrated" elements are an

answer. Possibly it will be found advantageous to build total subarrays with electronics and interconnecting networks both fabricated together. The subarray diminsions would be limited by technology's ability to produce the desired number of elements with a 100% yield. In connecting single source modules and subarrays extra connectors are necessitated by the connecting networks if this method is to be used, thus pushing cost up, not to mention introducing technological problems associated with connecting microstrip in a low Toss fashion.

The redeeming characteristic of the interconnecting circuits technique is its ability to perform a very close match over large scan angles. When used in a triangular grid array geometry it suitably connects the six adjacent elements (see Fig. 4-2).

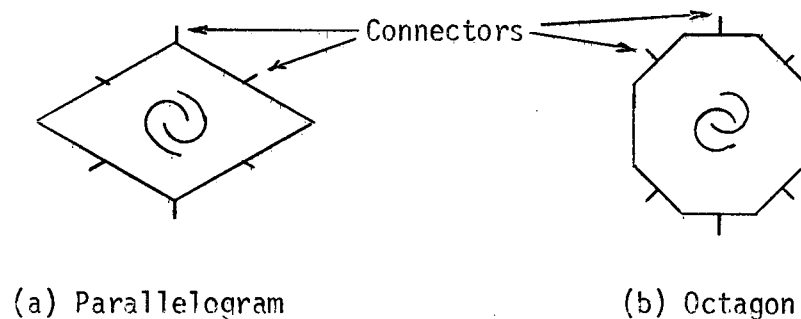(a) Parallelogram   (b) Octagon

Fig. 4-2. Array Modules for Use in 60° Triangular Grids.

The triangular grid array requires less elements than a square geometry to maintain a specified effective antenna aperture given the need for a specific scan cone with no grating lobes.

A. INTERCONNECTING CIRCUIT EFFECTS

Because of the mutual coupling between elements of a planar antenna array, the input impedance to each element varies with scan angle.. The ideal way to compensate for this effect would be to introduce some lossless circuit element into the line between the antenna and its generator (source) that varied with scan angle in a way to counteract the variations in input impedance due to mutual coupling effects, thus wide scan angle impedance matching could be accomplished. Hannan et al. [13] devised a method whereby a shunt susceptance introduced between adjacent antenna array elements varies a feed-back signal to each generator producing an approximate match. Because the elements are added in parallel shunt admittances rather than series impedances will be considered. Figure 4-3 shows three neighboring elements in an infinite linear array where an element is composed of an antenna, transmission line, and a generator.
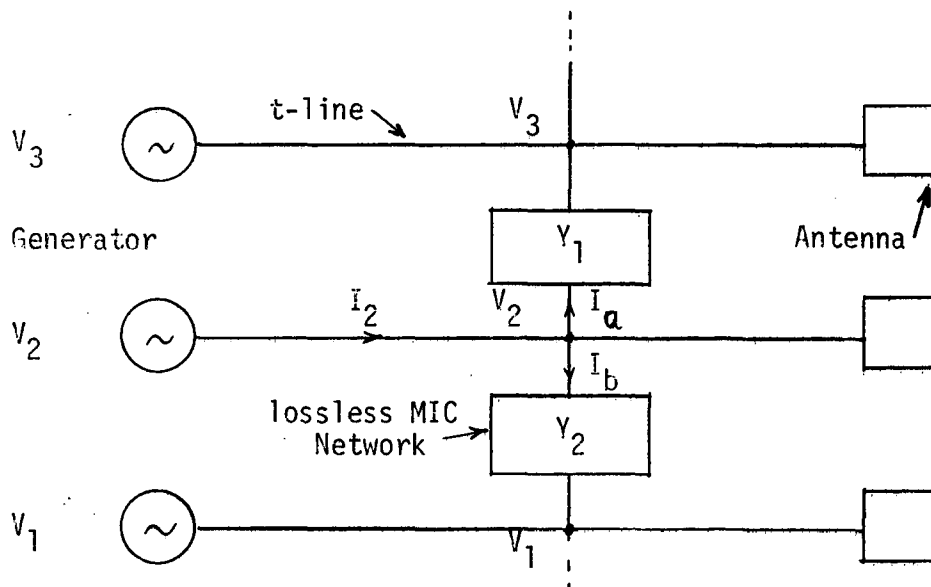

Fig. 4-3. Shunt Admittance Interconnection of Adjacent Array Elements

Start by considering an admittance

$$Y = G + jB$$

$$(G = \text{conductance}, \quad B = \text{susceptance})$$

placed between adjacent elements in a linear array. Currents I_a and I_b are assumed to flow in the directions shown in Fig. 4-3. Due to the two circuits adjacent to and connected to element #2 a net feedback current I_2 is felt at generator #2. The following development shows how this current is a function of the phase difference, δ, between adjacent elements in a linear array of identical elements. A similar development can be made for planar arrays in terms of row and column phase shifts. Referring to Fig. 4-3 it is seen that

$$I_2 = I_a + I_b \tag{4-2}$$

$$I_a = (V_2 - V_1)Y_1 \tag{4-3}$$

$$I_b = (V_2 - V_3)Y_2 \tag{4-4}$$

$$I_2 = Y_1(V_2 - V_1) + Y_2(V_2 - V_3) \tag{4-5}$$

Letting $Y_1 = Y_2 = Y$ and considering some equivalent admittance shunted to ground on element #2, then

$$Y_{eq.} = \frac{I_2}{Y_2} \tag{4-6}$$

$$Y_{eq.} = \frac{Y_1 (V_2 - V_1) + Y_2(V_2 - V_3)}{V_2} \tag{4-7}$$

$$Y_{eq.} = 2Y - Y \left(\frac{V_1}{V_2} + \frac{V_3}{V_2}\right) \tag{4-8}$$
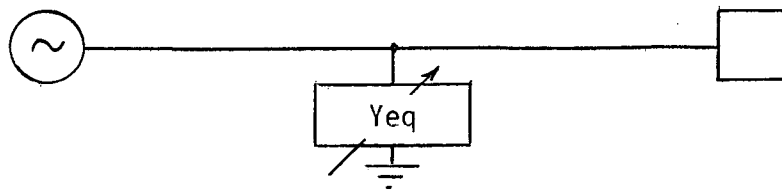
Fig. 4-4. Equivalent Admittance to Ground

But the elements are fed with equal amplitude sources with phases
differing by fixed increments.

$$V_1 = V_e^{j\psi_1}; \quad V_2 = V_e^{j\psi_2}; \quad V_3 = V_e^{j\psi_3} \qquad (4\text{-}9)$$

To steer a linear array in the $-\theta$ direction the phases in (4-9) are
given by [23]

$$\psi_1 = kd \sin \theta + \delta_1 \qquad (4\text{-}10a)$$

$$\psi_2 = kd \sin \theta + \delta_2 \qquad (4\text{-}10b)$$

$$\psi_3 = kd \sin \theta + \delta_3 \qquad (4\text{-}10c)$$

For equally spaced elements the progressive phase shift per element
is constant and it follows that

$$\delta_2 = 2\delta_1 \qquad (4\text{-}11)$$

$$\delta_3 = 3\delta_1 \qquad (4\text{-}12)$$

$$\delta_n = n\delta_1$$

Therefore from Eq. (4-8)

$$Yeq. = 2Y - Y[e^{j(\delta_1-\delta_2)} + e^{j(\delta_3-\delta_2)}] \qquad (4\text{-}13)$$

$$Yeq. = 2Y (1- \cos \delta) \qquad (4\text{-}14)$$

$$Yeq. = 4Y \sin^2(\delta/2) \qquad (4\text{-}15)$$

Thus if interconnecting admittances are used, the effect is equivalent to putting a shunt admittance to ground which varies as $4Y \sin^2(\delta/2)$ where δ = is the progressive phase shift per element. In order to determine the angle from broadside in which the beam is pointing, Eq. (4-10a) must be solved for $\psi_1 = 0$. The scan angle, θ, for a linear array given by

$$\theta = \sin^{-1}\left[\frac{-\delta_1}{kd}\right] = \sin^{-1}\left[\frac{-c\delta_1}{\omega d}\right] \qquad (4\text{-}16)$$

where

      d = spacing between elements

      c = speed of light

      ω = radian frequency

To aid in design a plot of $\sin^2(\delta/2)$ is given in Fig. 4-5.

The shunt susceptances can be put between adjacent elements to match the generator in both E-plane and H-plane scans. For the case of D-plane scan which is a linear superpostiton of simulataneous E and H-plane scan the admittance will vary as $4Y \sin^2(\delta/2\sqrt{2})$.
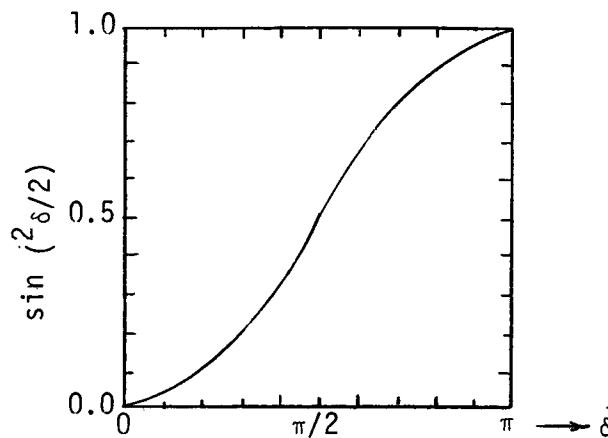

Fig. 4-5. Plot of $\sin^2(\delta/2)$

B. REALIZATION OF AN IMPEDANCE MATCH

If the input impedance to a one port network is known and it is desired to cancel the reactive portion, the series addition of the conjugate reactance is all that is necessary when the magnitude of this reactance is extremely small a combination L-C circuit will produce any magnitude of input reactance desired. Carter [22] has published a graph of experimental data on how the input impedance of a central element in a rectangular array of half-wave dipoles changes with scan angle. The geometry of the array is given in Fig. 4-6 and the impedance variations are given in Fig. 4-7. The variation in the resistive portion of input impedance is small and in its worst case is only twenty ohms over a 45° H-plane scan. However, for the H-plane scan of 45° the reactance increases from 26 ohms to 144 ohms. The matching techniques will be concerned only with the reactive portion in order to have maximum power transfer to the load.

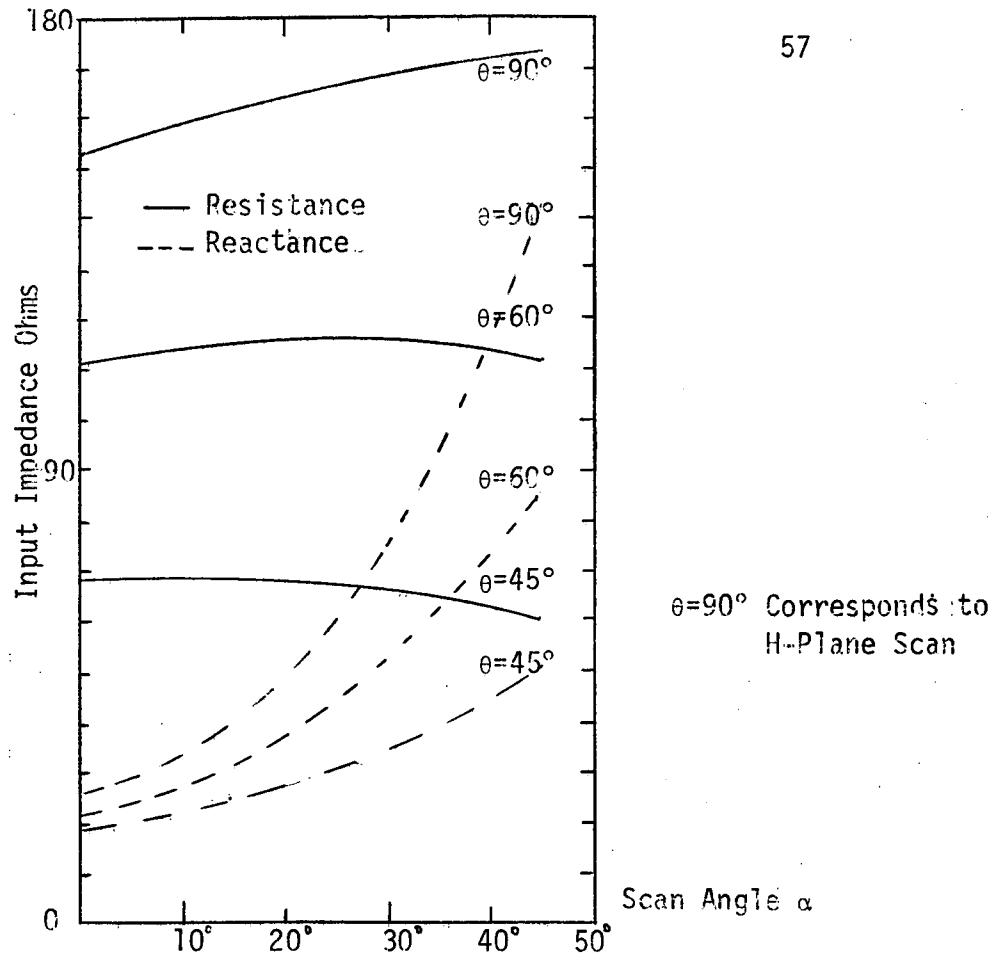Fig. 4-6. Array Geometry Giving Angle Criteria

Fig. 4-7. Variation of the Input Impedance of a Central Element of a
61 Element $\lambda/2$ Dipole Array Over a Ground Plane.

The spacing between the elements of the dipole array is a half
wavelength, therefore for H-plane scan ($\theta=90°$) the scan angle occurs
for a phasing between elements of δ_x.

$$\psi_x = kd_x \sin \alpha + \delta_x \qquad (4\text{-}10a)$$

The condition $\psi_x=0$ points the beam in the z direction. Solving for
δ_x gives

$$\delta_x = kd_x \sin\alpha = \frac{-2\pi}{\lambda} \frac{\lambda}{2} \sin \alpha \qquad (4\text{-}17)$$

$$\alpha = \sin^{-1} \left(\frac{-\delta_x}{\pi}\right) \qquad (4\text{-}18)$$

Scan angle	Phase	Before Match Input Impedance		$4 \sin^2(\delta_x/2)$	After Match Input Impedance	
α	δ_x	Z_{in}	$\lvert Z_{in} \rvert$		Z_{in}	$\lvert Z_{in} \rvert$
0°	0	153+j26	155.4	0.0	153	153
30°	-90°	170+j75	185.8	2.0	153-j5.3	153.1
45°	-127°	172+j143	223.6	3.1	153	153

Table 4-2. Data Necessary for Matching H-Plane Scan

When the input impedances for the scan angles are known as given in Fig. 4-7 then the H-plane can be matched with the aid of a Smith Chart. The following steps are illustrated in Fig. 4-8.

1. Choose the broadside impedance as a normalization factor and convert it to pure resistance. This meant in our example a series addition of -j26.

2. Normalize all other impedances with the broadside impedance. For our example $Z_0 = 153$ ∴ all Z_{in}/Z_0 so we can enter the chart.

3. Convert all impedance points to admittance points.

4. Rotate the admittance locus to a curve of constant conductance this is accomplished by adding series t-lines. Notice: the locus always rotates toward the generator.

5. The equivalent susceptance Beq. needed for $\Gamma=0$ is seen graphically to be $-.8Z_0$ for our example. However, we have shown in Eq. 4-15 that this can be solved by adding a shunt susceptance of $B = \dfrac{Beq}{3.1} = -.258 \ Z_0$

a) Enter Normalized
   Impedance Locus

b) Convert to
   Admittance Locus

$L = .238\lambda$

c) Rotate Locus Clockwise to
   Circle of Constant Conductance
   by Adding a Length L of t-line.
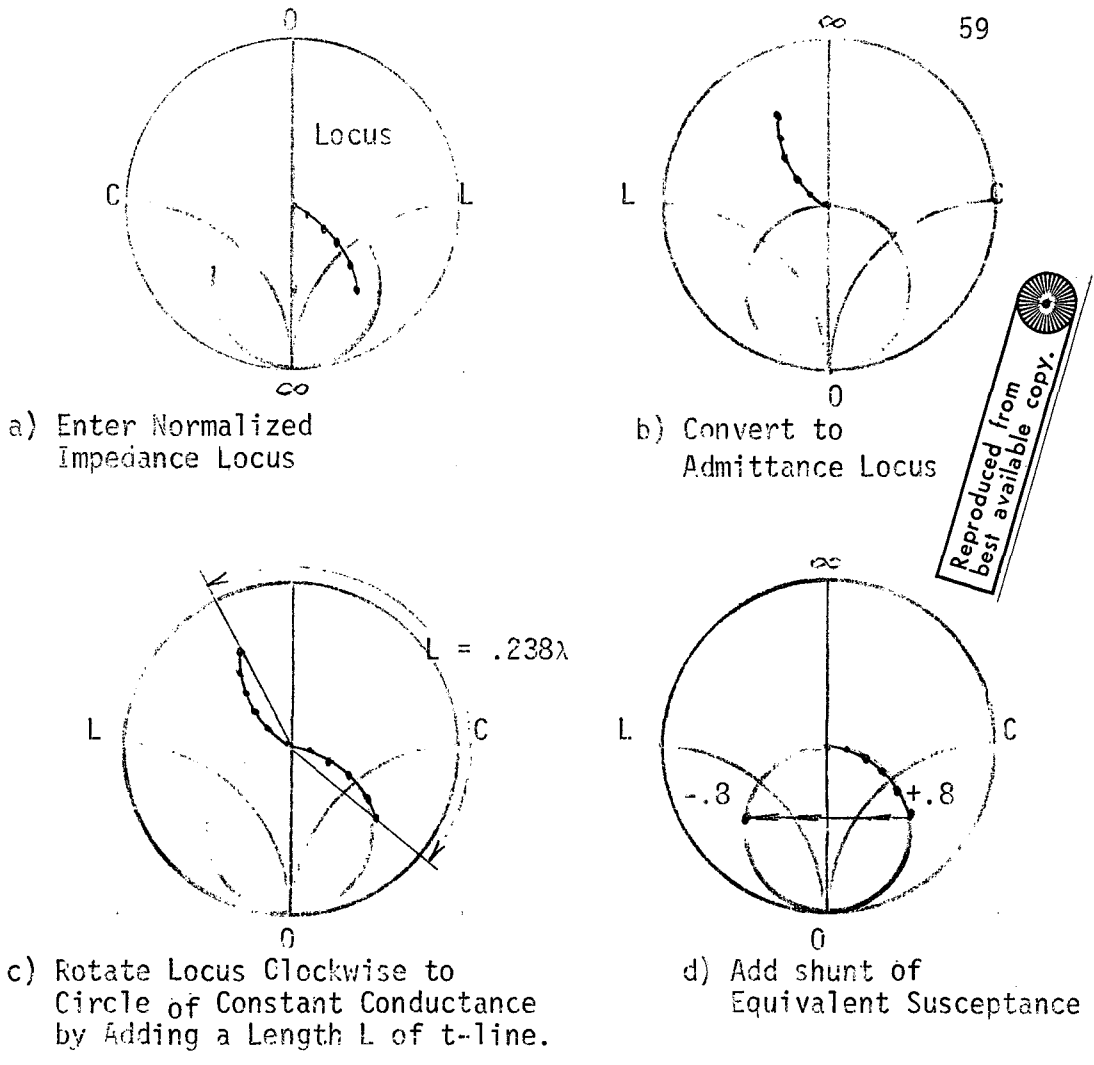
d) Add shunt of
   Equivalent Susceptance

Fig. 4-8. Graphical Analysis of Impedance Matching Technique.

In order to obtain the results given in the last column of Table
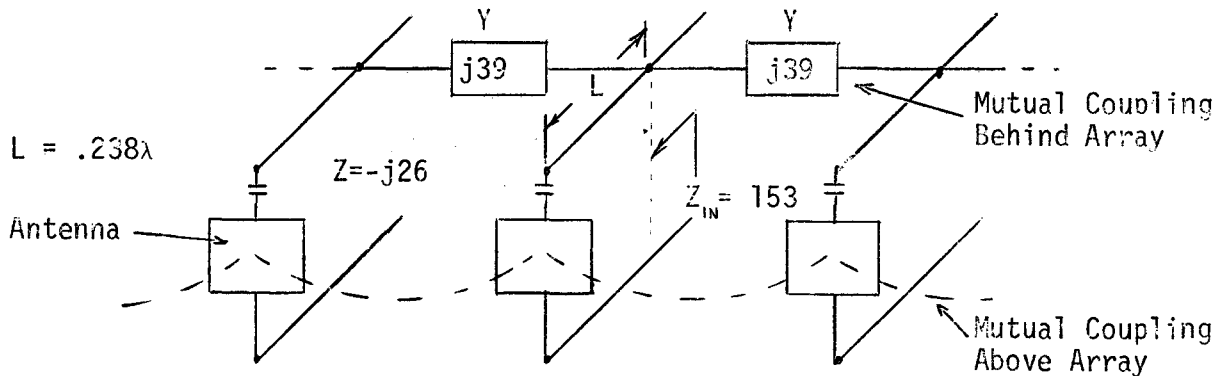4-2 the circuit of Fig. 4-9 must be implemented.

Y $j39$ L   Y $j39$

Mutual Coupling
Behind Array

$L = .238\lambda$ $Z = -j26$ $Z_{IN} = 153$

Antenna

Mutual Coupling
Above Array

Fig. 4-9. Equivalent Circuit for H-Plane Scan Impedance Matching of an
          Array Characterized by Data Given in Fig. 4-7.

C.   REALIZATIONS USING MICROSTRIP COMPONENTS

Once the equivalent values of admittance have been determined by the
methods of Section 4-2 the components can be fabricated using MIC techniques.
In the example just given a susceptive admittance of -39.5 ohms is
necessary. At a frequency of 2.5 GH_z and if a single component is used,
this value corresponds to an extremely small inductance of 1.61
picohenrys or a 24 mil length of 50 Ω microstrip on 24 mil thick alumina.
This value is impractical. However, small "effective" inductances and
capacitances can often be obtained using parallel or series L-C net-
works composed of realizable L's and C's. The common L-C tank circuit
is an example of this and is seen in Fig. 4-10 along with its properties.
In Fig. 4-11 the admittance versus frequency characteristics of a series
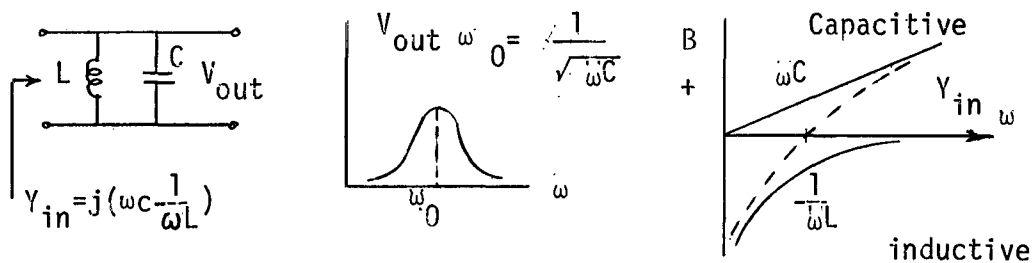L-C network are illustrated.

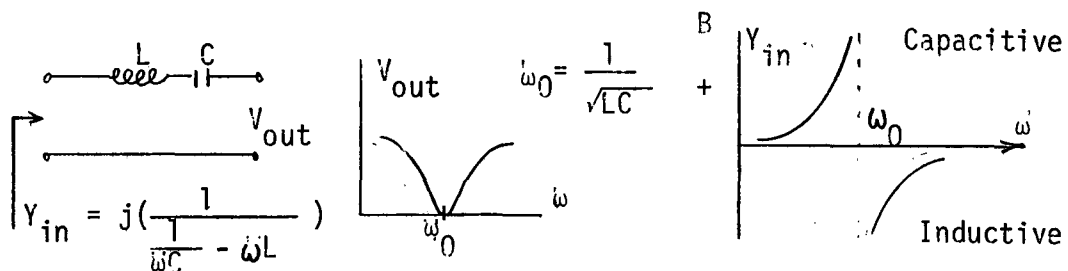Fig. 4-10. Properties of a Circuit with Parrallel L and C.

Fig. 4-11. Frequency Characteristics of a Series L-C Network

The equation for the input admittance of the circuit of Fig. 4-10(a) is

$$Y_{in} = jB = j(\omega C - \frac{1}{\omega L})$$ (4-19)

where B is the susceptance. Returning to the example, a value of B = -39.5 is required. If Eq. (4-19) is solved for L given any C and using the parallel L-C network, it will turn out that the value of L is again too small to be practical. When a series L-C circuit is used the input admittance is

$$Y_{in} = jB = j\ \frac{1}{\frac{1}{\omega C} - \omega L}$$ (4-20)

Choosing a value of 1.0 nanohenry for L to achieve a value for B = -39.5 the value of C is 4.07 picofarads. All of these values are parctical and have been built in usable microwave integrated circuits [18]. The capacitor with a value of 4.07 picofarads can be constructed as a lumped element by the classical method of dielectric separated metal sheets or the interdigital capacitor. Section 4-4 contains the theoretical work by Alley [14] on the interdigital capacitor. Also curves are given which can be used to determine the parameter values necessary to construct the capacitor. If the antenna elements are modular a portion of the necessary capacitance could be put into each module as depicted in Fig. 4-12
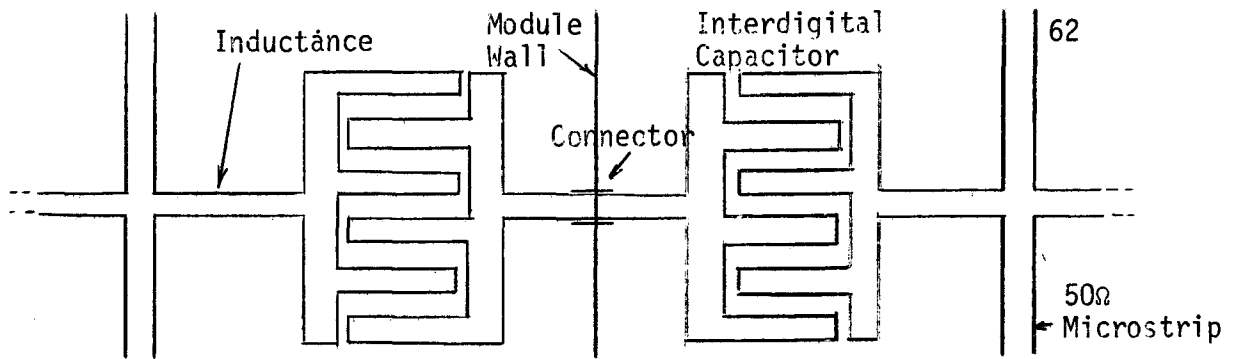
Fig. 4-12. Interdigital Capacitor for Use in Modular Antenna Elements

The value of the capacitance of each capacitor will be 8.14

picofarads. Using Eq. 4-21 and Fig. 4-15 the necessary parameters

can be determined. The results are: $X = 2$ mil, $N = 20$, $\ell = 30.2$ mil,

$w = 158$ mil, $\varepsilon_r = 10$. Refer to Fig. 4-13 for interpretation of these

values. However, had the capacitor of Fig. 3.6 been used with SiO_2 as

the dielectric. for a spacer 1 μm thick,the value of 8.14 picofarads

would require a surface area of 389 mil^2 whereas the IdC needs 4740

mil^2. This area is obviously less than the interdigital capacitor.

The production of a metal sandwich capacitor requires more steps and

in thus costlier. The inductor values can be obtained from Eq.(3-1)

or Eq. (3-4) and are realized from the lengths of T-line connecting

the capacitor between elements. The parasitic capacitance of the

interdigital capacitor has a value of 2.14×10^{-14}f and is not

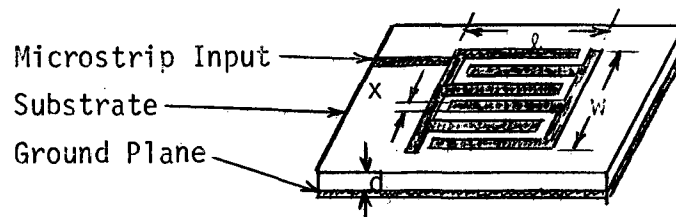considered.

D.   THE INTERDIGITAL CAPACITOR

Fig. 4-13. The Interdigital Capacitor on Dielectric of Thickness d

Above a Ground Plane.

The interdigital capacitor can be used as a lumped element interconnecting circuit element if the capacitive values required fall in the range 0.1 to 10.0 picofarads.
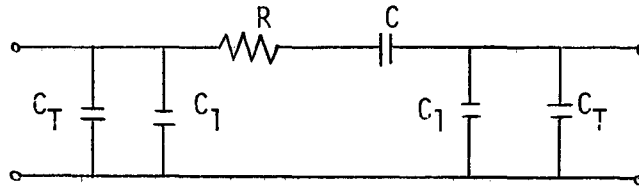

Fig. 4-14. Equivalent Circuit for the Interdigital Capacitor

The terminal strip capacitance C_t and the finger parasitic capacitance are much less than the value of C. The important restriction being that C_1 and C_t can be neglected if the capacitor-frequency product falls below 2×10^{-3}. The value for the capacitance C has been analyzed by Alley [14] and his formula for C is

$$C = \frac{(\epsilon_r+1)}{W} \ell \ [(N-3) \ A_1 + A_2] \ \text{picofarads} \qquad (4-21)$$

where
W = width of terminal strips in inches
ℓ = length of finger in inches
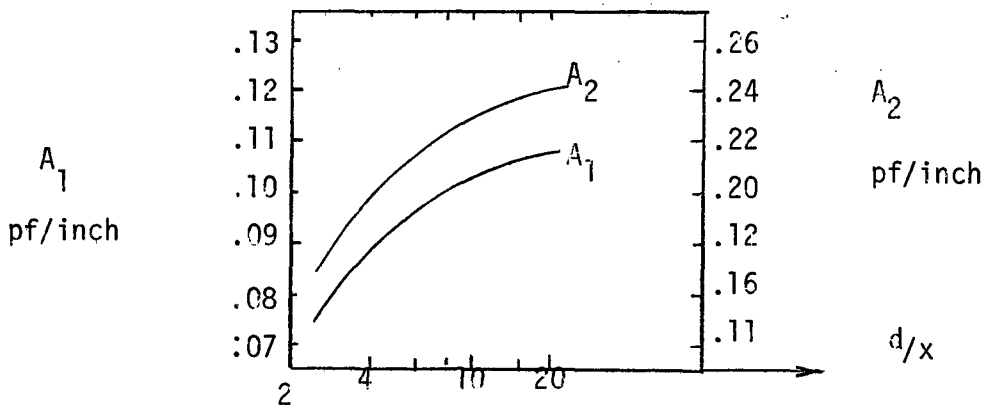ϵ_r = relative dielectric constant

Fig. 4-15. Computational Graph for Determination of A_1 and A_2 Given the Dielectric Thickness d and Finger Separation X.

The prediction of the capacitive value from Eq. (4-21) is subject
to the restraint that the width of the fingers and the separation of the
fingers is identical. The series resistance R forms a resonant circuit
with C_1 and C_t which can be treated as some total parasitic capacitance
and the effect of this filter circuit should be avoided. The series
resistance is a function of the sheet resistance and is given by:

$$R = \frac{1.333 \, \ell \, R_s}{XN} \qquad (4-22)$$

where R_s is the sheet resistance. For gold plated conductors four skin
depths thick the sheet resistance is $1.5 \times 10^{-6}\sqrt{f}$. The total parasitic
capacitance can be approximated using the surface area of the capacitor
and Eq. (3-6). With these values known the problem of the resonant
circuit can be avoided.

The quality factor of this capacitor is given by:

$$Q = \frac{Q_c Q_c}{Q_c + Q_d} \qquad (4-23)$$

where Q_c is the quality factor associated with the conductor and Q_d
is associated with the dielectric.

$$Q_c = \frac{0.75 \, NX}{\omega C \, \ell \, R_s} \qquad (4-24)$$

and

$$Q_d = \frac{1}{\tan \theta} = \frac{1}{\text{dielectric loss tangent}} \qquad (4-25)$$

The interdigital capacitor is acting as a lumped element even
though it is above a ground plane and thus it can be fed directly by
a distributed microstrip transmission line. Another attractive

F

characteristic is its trim capability, providing that in the inital fabrication additional fingers are produced. This along with simultaneous one step production reduces costs.

CHAPTER V

POWER LIMITS AND WIDE-BAND BALUN FEEDING OF A SPIRAL ANTENNA

For a planar array which is designed for wide scan angles the ideal array element would have a nearly hemispherically isotropic pattern and operate well in an array environment. Many airborn and spacecraft systems utilize circular polarization so antenna alignment between transmitter and receiver is not critical. If an array is to handle a large number of channels or have a multimode, multispectral capacity, the element should also have constant characteristics over a large bandwidth. All these features are obtained with the spiral antenna which has a comparatively large beam width with a polarization axial ratio close to one. Frequency bandwidths of approximately 2:1 are common for spiral antennas. Bawer and Wolfe [24] have published experimental data for a typical spiral antenna, the results of which are summarized in Fig. (5-1). From Fig. (5-1) it is clear the spiral antenna is only approximately frequency independent, however, it should be adequate for most wide band applications.

A spiral antenna which is compatable with MIC technology is amenable to flush mounting in the array surface, and its mass is small compared to other antennas which generate circular polarization. In order for the spiral to radiate in a well behaved fashion a high turn density is recommended. However, power considerations set a limit since they require enough spacing between arms to avoid voltage breakdown. Therefore, a

tradoff must be determined between the number of turns made by a spiral arm and maximum power radiation desired. When complementary symmetry used, the spacing between arms equals the width of the conductor forming the arm. Usually the spiral arms are terminated in some form of dissipating load to avoid the generation of spurious modes due to reflection. Continuous power per element should not exceed nine watts for an 18 GH_z spiral etched from gold clad alumina and designed with six turns and 2:1 bandwidth.
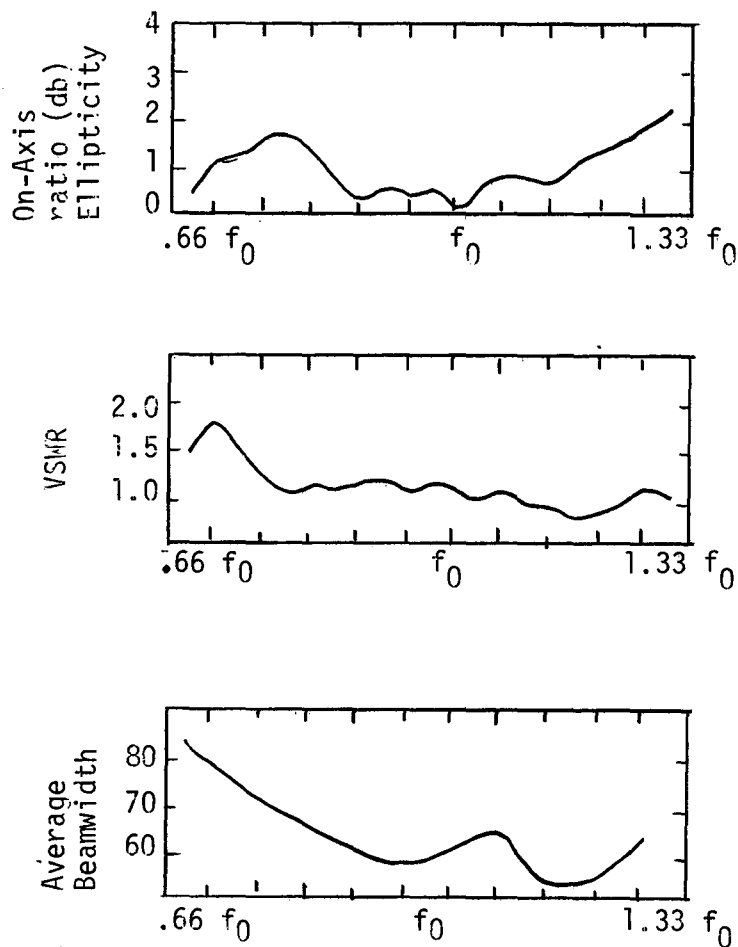

Fig. 5-1. Characterestics of an Archimedian Spiral Antenna Designed with a Center Frequency of f_0.

Two alternatives of feeding a wideband spiral in the normal mode
(i.e. current 180° out of phase at the feed) from an unbalanced
transmission line are investigated. The Bawer balun has its worst
impedance match in the operating band at the center frequency. It
also requires two sides of etched microstrip for realization. The
Craven balun in also matched at the extremes of its operating band,
but it is matched at the center frequency also. Spiral antennas when
put in an array environment normally are placed one quarter wavelength
above a ground plane to eliminate back radiation and provide shielding.
The construction of the Craven balun is such that its ground plane can
serve the above purposes as well as its transformer function. Its
feed lines run directly from the MIC network to the center balanced
feed of the spiral, and this balun is thought best suited for X-band
and above spiral feeds.

A.   POWER LIMITS

The maximum power handling capability of the spiral antenna will
be a function of the RF voltage breakdown between the conductors and
the maximum allowed current flow through the conductors. Once the
input impedance is known the maximum power the antenna element can
radiate will be determined by which occurs first, voltage breakdown
or excessive current causing subsequent failure due to overheating.

In the case of a dc voltage between two parallel plates in dry
air at standard pressure the electric field intensity necessary for
breakdown is 30,000 volts/cm [29]. When a high frequency voltage is
impressed between the conductors the electric field producing

breakdown is less. How much less depends on the field configuration

resulting from the applied RF voltage. In the case of conductors

interfaced by air on one side and a dielectric on the other, the

electric field will be altered thus increasing the electric field

in the air. The breakdown voltages versus conductor spacing with

frequency as a parameter are empirically given in Fig. 5-2 for

two plates in dry air at one atmosphere pressure (14.7 psi or 760
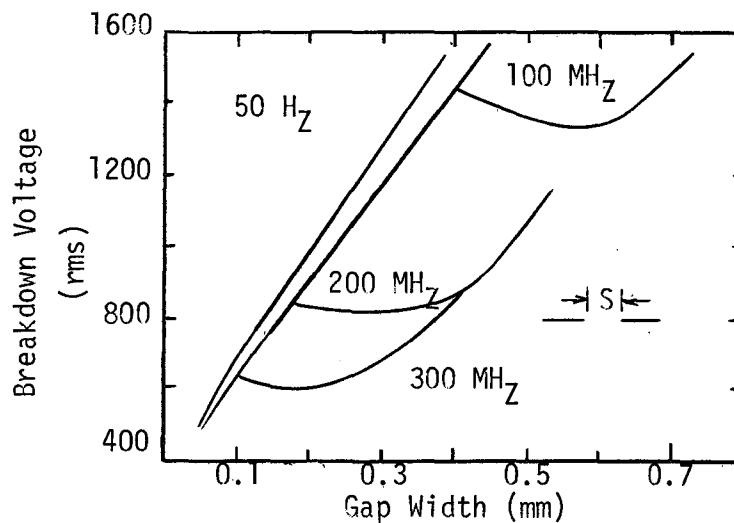
mm Hg).

Fig. 5-2. Variation of Breakdown Voltage vs. Conductor Spacing as a
Function of Frequency [15].

If the spiral antenna is designed to operate at a center frequency,
f_0, of 18 GH_z, the free space wavelength is 1.669 cm. Using the band
theory approximation for spiral [24], most of the radiation occurs at
a circumference of one wavelength which at 18 GH_z gives

$$C = \pi D = 1.668 \text{ cm.} \qquad (5-1)$$

Available data on the spiral antenna has shown that the supporting

dielectric substate has little effect in reducing the electrical size of

the antenna and phase velocity of the two wire balanced transmission line that forms the antenna. Thus the wavelength of the RF energy is not significantly different from that of free space. Therefore, the diameter of a spiral with a 2:1 bandwidth and f_0 = 18 GH_z is 0.795 cm.

Let us consider an Archimedian spiral illustrated in Fig. 5-3. Its defining equation is given by

$$r = A\theta + S \qquad (5-2)$$

r = radius from a point on an arm to center

A = growth constant

S = orgin constant
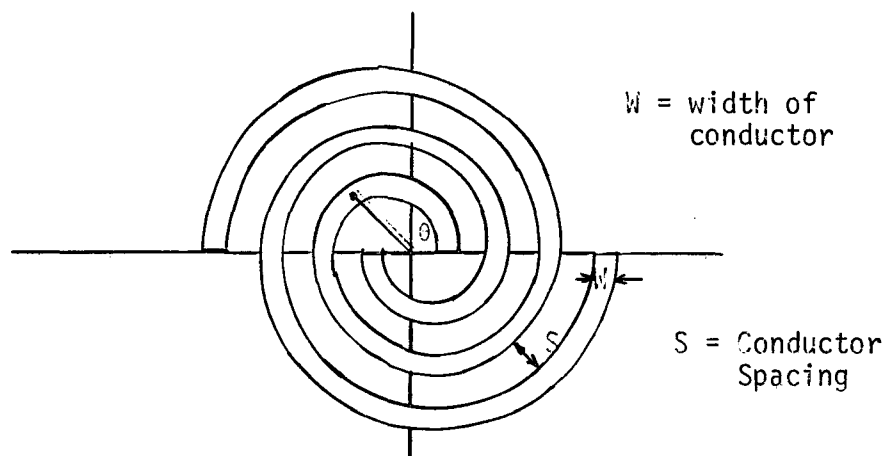
θ = polar angle in radians

Fig. 5-3. 1.5 Turn Archimedian Spiral Antenna

The input impedance to a complementary antenna has been shown to be 189 ohms [25]. In order for the spiral antenna to approximate a complementary antenna the conductor width should equal to the spacing. Applying this condition, Eq. (5-2) becomes:

$$r = s\left[\frac{2\theta}{\pi} + 1\right] \qquad (5-3)$$

The value of the conductor spacing S will be a design criteria determined by the number of spiral arm turns N. Thus the spacing S in terms of the spiral diameter becomes:

$$S = \frac{D}{8N + 2}$$ (5-4)

For the case of a six turn, 18 GH_z spiral the spacing S is 0.159 mm. Assuming the breakdown in air occurs for a field strength of 30 kv per cm. and using a safety factor of 2.4, a maximum of approximately 200 volts is possible between conductors. This corresponds to a maximum possible current flow which is on the order of one ampere since the input impedance is approximately 189 ohms. It is also necessary to theoretically determine the maximum current density which can be tolerated by the metal spiral arms. The following parameters must be considered:

1. Conductor resistivity ρ

2. Conductor cross-sectional area

3. Thermal properties of adjacent media

4. Conductor melting point

5. Joule heating of conductor

6. Specific heat of conductor and media

7. Operating frequency (skin effect)

To avoid the problem of theoretically evaluating the above for the maximum current carrying capacity I_{max}, an approximate I_{max} can be found by considering the current limitations of specific conductors given their cross sectional area.
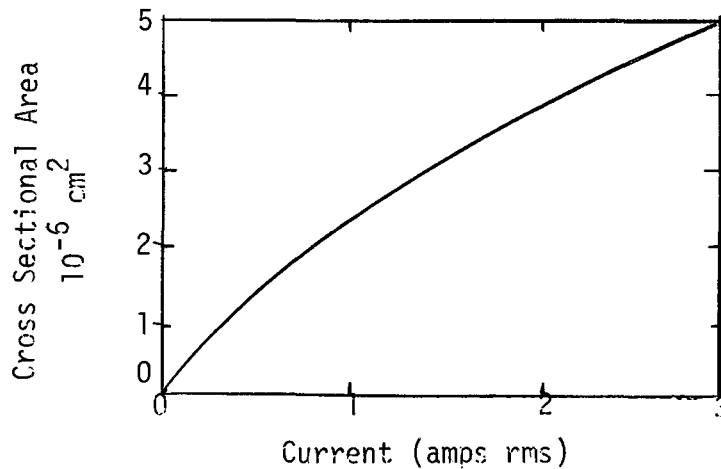
Fig. 5-4. Maximum Current Capability of Copper Wire (Cu melting point 1080°C)

For a microstrip spiral the conductor thickness is usually 3.8-5.0 micrometers or about ten skin depths at 18 GH_z. However, the current will see àn effective conductor thickness of 4.1×10^{-5} cm due to the skin effect. The metalization is a combination of silver and gold which melts round 1000°C and will support a maximum current density of 5×10^5 amps/cm^2. The conductor width is 1.59×10^{-2} cm. and thus has a cross sectional area of 6.5×10^{-7} cm^2. This leads to a figure of 325 ma. for I_{max}. After applying a safety factor of two an 18 GH_z complementary microstrip spiral antenna mounted on alumina can radiate 8.5 watts of continuous rms power per element which is much less than the maximum power limit set by considering voltage breakdown in air. The evaluation of peak pulse power in terms of breakdwon voltage alone is allowable provided the duty cycle is small enough to restrict critical ion accumulation. Note that spacecraft applications present an entirely new problem where material outgassing at low pressures may produce breakdown at considerably lower values then in air. Using a breakdown voltage safety factor of 100 would give a power limit of about 4 watts per element which is a confortable margin compared to the low powers produced by the sources that might be used at this frequency.

B.   BALUN FEEDING OF THE SPIRAL ANTENNA

A balun is a transformer which performs matching between balanced
and unbalanced transmission lines. In spiral MIC applications the balun
is an interface between the balanced spiral feed and the unbalanced
microstrip t-line. The microstrip circuitry is usually designed using
the maximum quality factor 50 ohm t-line whereas the spiral input
impedance for complementary symmetry is around 189 ohms. It is
desirable to have the magnitude of the spiral's impedance closer
to the microstrip impedance to avoid large power reflection. It
is speculated that increasing the conductor width-to-spacing ratio
to greater than unity decreases the dual-arm spiral antenna's input
impedance. Because the spiral is used in wideband applications the
balun should also be wideband. Consider the input impedance of the
transmission line network of Fig. 5-5 [27]. The input is a coaxial
t-line and the output is a twin line utilizing the shielding of the
two coaxial lines. The theory is developed in terms of balanced
and unbalanced lines such that a substitution of microstrip t-line
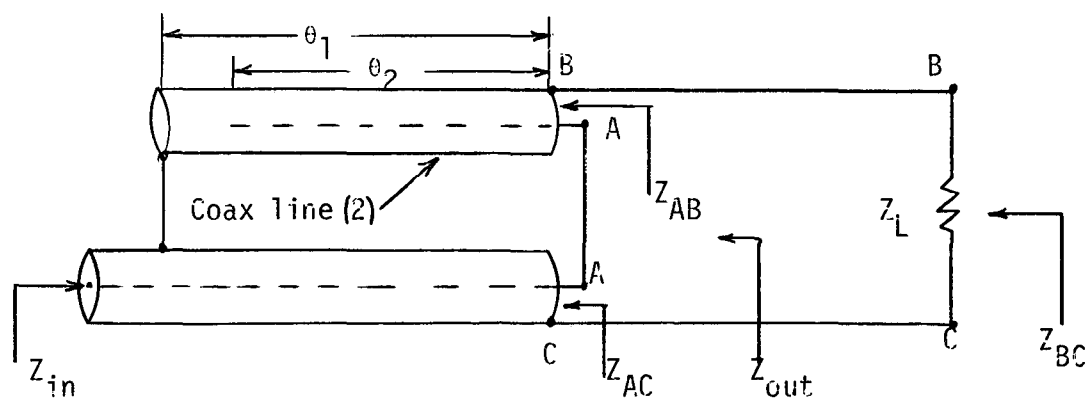parameters is obvious.

Fig. 5-5. Wide Band Balun

Using nodal analysis we can express the impedance Z_{AC} as:

$$Z_{AC} = Z_{AB} + Z_{Bc} \qquad (5-5)$$

implying:

$$Z_{AC} = Z_{AB} + \frac{Z_{out} Z_L}{Z_{out} + Z_L} \qquad (5-6)$$

The input impedance to an open circuit t-line with characteristic impedance Z_u^i is:

$$Z_{AB} = -j Z_u \cot \theta_2 \qquad (5-7)$$

For a short circuited t-line of impedance Z_b the input impedance is:

$$Z_{out} = j Z_b \tan \theta_1 . \qquad (5-8)$$

Substituting Eq. 5-7 and Eq. 5-8 into Eq. 5-6 we get:

$$Z_{AC} = \frac{R_L Z_b^2 \tan^2 \theta_1 + j Z_b \tan \theta (R_L^2 + X_L^2 + X_L Z_b \tan \theta_1)}{R_L^2 + (X_2 + Z_b \tan \theta_1)^2} - j Z_u \cot \theta_2 \qquad (5-9)$$

where

R_L = Real part of the load impedance

X_L = Imaginary part of the load impedance

Z_b = Characteristic impedance of the balanced T-line

Z_u = Characteristic impedance of the unbalanced d T-line

θ_1 = Electrical length of twin line to short in radians

θ_2 = Electrical length of coaxial line to open in radians

In order to draw conclusions from Eq. 5-9 the following pedagogical approximations are made: $X_2 = 0$, $\theta_1 = \theta_2 = \theta$, and $Z_u = Z_b$. The result

is $Z_{in} = Z_{AC}$ (i.e. a perfect impedance match at the frequencies corresponding

to θ which solve the equation $\sin^2\theta = Z_{in}/R_L$). For $\theta = 90°$ the length

of t-line (2) is one quarter wavelength at f_0 and thus at the frequency

f_0, $Z_{AC} = Z_L$. Obviously, the center frequency, f_0, has the highest

reflection of power of all frequencies in the operating band, and in the

case where $Z_{in} = 50\Omega$ and $R_L = 189\Omega$ an auxillary impedance transformer

is needed. A tappered line will suffice. To increase the bandwidth

of the balun the condition $Z_u = R^2_L/Z_b$ should replace $Z_u = Z_b$. A

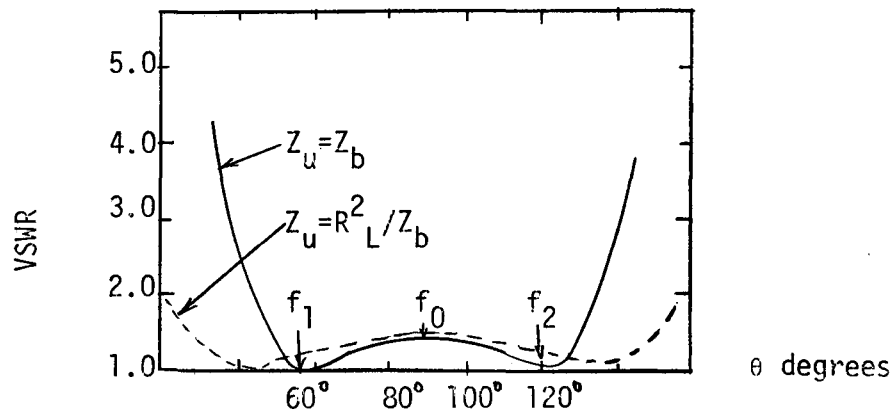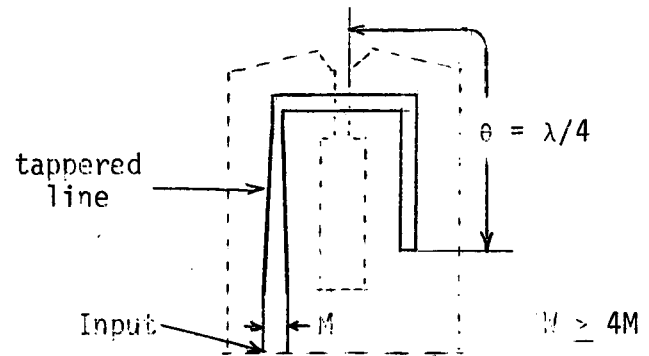comparison of these two choices is illustrated in Fig. 5-6.

Fig. 5-6. Graphical Interpretation of Eq. 5-9 with $X_L = 0$ and $\theta_1 = \theta_2 = \theta$.

Frequencies f_1 and f_2 Correspond to Solutions of $\sin^2\theta = Z_{in}/R_L$

The spiral antenna is usually mounted over a cativity which is a

quarter-wavelength deep at the center frequency. This places a dimensional

restriction on the balun which is mounted perpendicular to the spiral

surface. Bawer and Wolfe [16] applied Robert's technique to microstrip

transmission line. The microstrip balun is illustrated in Fig. 5-7.
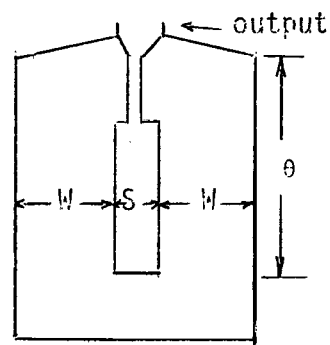
a) Ground plane and balanced output   b) unbalanced microstrip input

Fig. 5-7. Bawer and Wolfe Printed Circuit Balun.

The necessary parameter values for constructing the desired micro-strip input impedance and taper (impedance transformer) are given in Chapter II. The impedances can be calculated using Eq. 2-57. The characteristic impedance for the balanced transmission line has been empirically determined [16] and is listed in Fig. 5-8.

W/S	Z_0 (ohms)
2	220
4	185
6	170
8	160
10	155

Fig. 5-8. Characteristic Impedance for a Two Ribbon Balanced Line

The most undersireable characteristic of the Bawer balun concerns the large impedance mismatch resulting about its design center frequency. On the other hand, the microstrip meander line phase shifter when used with the broad-band phase shifting properties of coupled microstrip results in a balun technique with a relatively frequency independent impedance characteristic. Negligible VSWR at the center frequency; and normal mode excitation are achieved using this method. Craven [17] using the method of Schiffman [28] utilized this method of balun design,but Craven's balun unnecessarily occupys a large area. A more optimum balun design using microstrip t-lines is illustrated in Fig. 5-9. The broad-band 90° phase shifters have less than a four degree phase deviation over a 2:1 bandwidth. Figure (5-10) is a Shiffman type-A network. The phase shift ϕ of coupled microstrip is given by

$$\phi = \cos^{-1} \frac{\dfrac{Z_{oe}}{Z_{oo}} - \tan^2 \theta}{\dfrac{Z_{oe}}{Z_{oo}} + \tan^2 \theta} \tag{5-10}$$

where

Z_{oe} = characteristic impedance of one line to ground when equal in phase currents flow in both lines

Z_{oo} = characteristic impedance of one line to ground when equal out-of-phase currents flow in both lines

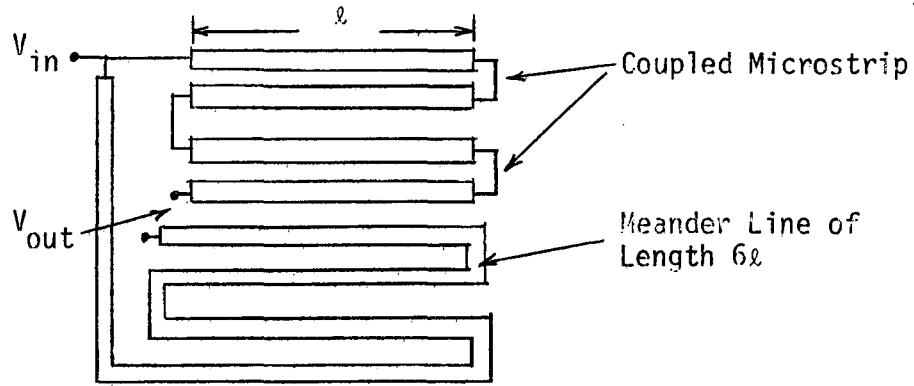$\theta = \beta\ell$ = electrical length of a uniform line length ℓ and phase constant β.

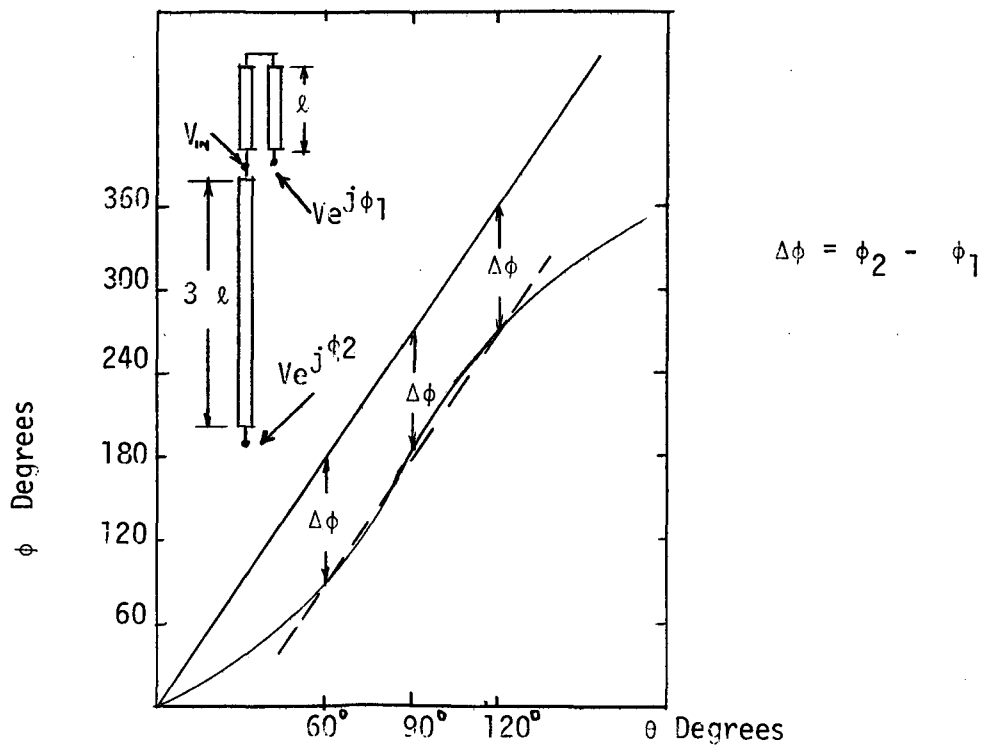Fig. 5-9. Coupled Microstrip Balun.

$$\Delta\phi = \phi_2 - \phi_1$$

Fig. 5-10.   90° Broad-Band Phase Shifter

The input impedance Z_{cm} to the coupled microstrip line is given by

$$Z_{cm} = \sqrt{Z_{oo} Z_{oe}} \qquad (5\text{-}11)$$

and the input impedance at the output port is independent of frequency and

is the series sum of the impedance of the uncoupled microstrip Z_0 and Z_{cm}.

The use of Fig. 2-2 will aid in the design of the coupled microstrip.   The

input impedance to the balun will be the parallel sum of the impedances Z_0 and

Z_{cm}.

REFERENCES

[1] Wheeler, H. A., "Transmission-Line Properties of Parallel Strips
     Separated by a Dielectric Sheet," IEEE Trans. on Microwave Theory
     and Techniques, Vol. MTT-13, March 1965, pp. 172-185.

[2] Assadourian, F. and Rimai, E., "Simplified Theory of Microstrip
     Transmission Systems," Proceedings of the I.R.E., December 1952,
     pp. 1651-1657.

[3] Judd, S. V., et al. "An Analytical Method for Calculating Micro-
     strip Transmission Line Parameters," IEEE Trans. on Microwave
     Theory and Techniques, Vol. MTT-18, No. 2, Febuary 1970, pp. 78-87.

[4] Cohn, S. B., "Shielded Coupled-Strip Transmission Line," IRE Trans.
     on Microwave Theory and Techniques, October 1955, pp. 29-38.

[5] Hilberg, "From Approximations to Exact Relations for Characteristic
     Impedances." IEEE Trans. on Microwave Theory and Techniques, Vol.
     MITT-17, May 1969, pp. 259-265.

[6] Bates, R. H. T., "The Characteristic Impedance of the Shielded Slab
     Line," IRE Trans. on Microwave Theory and Techniques, January 1956,
     pp. 28-33.

[7] Hyltin, T. M., "Microstrip Transmission on Semiconductor Dielectrics,"
     IEEE Trans. on Microwave Theory and Techniques, Vol. MTT-13,
     November 1965, pp. 777-781.

[8] Green, H. E., "The Numerical Solution of Some Important Transmission-
     Line Problems," IEEE Trans. on Microwave Theory and Techniques,
     Vol. MTT-13, September 1965, pp. 676-692.

[9] Yamashita, E. and Mittra, R., "Variational Method for the Analysis
     of Microstrip Lines," IEEE Trans. on Microwave Theory and Techniques,
     Vol. MTT-16, April 1968, pp. 251-256.

[10] Terman, F. E., Radio Engineer's Handbook. New York: McGraw-Hill,
     1943.

[11] Caulton, M. and Sobol, H., "Microwave Integrated-Circuit Technology-
     a Survey", IEEE Journal of Solid-State Circuits, Vol. SC-5, No. 6,
     December 1970, pp. 292-302.

[12] Lehrfeld, S. S., "What if You Don't Use Alumina?" Microwave, March 1971, pp. 54-56.

[13] Hannan, P. W., et al., "Impedance Matching a Phased-Array Antenna Over Wide Scan Angles by Connecting Circuits," IEEE Trans. on Antennas and Propagation, January 1965, pp. 28-34.

[14] Alley, G. D., "Interdigital Capacitors and Their Application to Lumped-Element Microwave Integrated Circuits", IEEE Trans. on Microwave Theory and Techniques, December 1970, pp. 1028-1033.

[15] Meek, J. M., and Cragge, J. D., Electrical Breakdown of Gases, Oxford University Press, London, 1953, pp. 381.

[16] Bawer, R. and Wolfe, J. J., "A Printed Circuit Balun for Use with Spiral Antennas," IRE Trans. on Microwave Theory and Techniques, May, 1960, pp. 319-325.

[17] Craven, J. H., "A Novel Broad-Band Balun", IRE Trans. on Microwave Theory and Techniques, November 1960, pp. 672-673.

[18] Sobol, H., "Application of Integrated Circuit Technology to Microwave Frequencies," Proc. IEEE, Vol. 59, August 1971, pp. 1200-1211.

[19] M. Caulton, B. Hershenov, S. Knight, and R. DeBrecht, "Status of Lumped Elements in Microwave Integrated Circuits-Present and Future," IEEE T-MTT, Vol. MTT-19, July 1971, pp. 588-599.

[20] S. B. Cohn, "Slot-Line an Alternative Transmission Medium for Integrated Circuits," IEEE G-MTT Int. Microwave Symp. Digest, May 1968, pp. 104-109.

[21] C. P. Wen, "Coplanar Waveguide, a Surface Strip Transmission Line Suitable for Nonreciprocal Gyromagnetic Twill Applications," IEEE G-MTT Int. Microwave Sump. Digest., May 1969, pp. 110-114.

[22] Carter, P. S., Jr., "Mutual Impedance Effects in Large Beam Scanning Arrays', IRE Trans. on Antennas and Propagation, May 1960, pp. 276-285.

[23] Dudgeon, J. E., "Effieiency and Efficiency Improvement Through Compensation," Technical Report No. 1, NAS8-25894, October 1970.

[24] Bawer, R. and Wolfe, J. J., "The Spiral Antenna", IRE Convention Record, 1960, pp. 87.

[25] Rumesy, V. H., _Frequency Independent Antennas_, Academic Press, New York, 1966, pp. 27.

[26] Bolz and Tuve, _Handbook of Tables for Applied Engineering Science_, CRC, 1970.

[27] Roberts, W. K., "A New Wide-Band Balun, " _Proceedings of the IRE_, December, 1957, pp. 1628-1631.

[28] Schiffman, B. M., "A New Class of Broad-Band Microwave 90-Degree Phase Shifters," _IRE Trans. on Microwave Theory and Techniques_, April, 1968, pp. 232-237.

[29] Southworth, G. C., _Principles and Applications of Waveguide Transmission_, D. Van Nostrand, New York, 1950.